J Therm Spray Tech
https://doi.org/10.1007/s11666-024-01894-1

ORIGINAL RESEARCH ARTICLE

Wear and Corrosion of HVAF and HVOF-Sprayed WC-CoCr Coatings on Aluminum Alloy

Tunji Adetayo Owoseni[1] · Mohit Gupta[1] · Shrikant V. Joshi[1] · Mare Ingmar[2] · Tommi Varis[3]

Submitted: 31 July 2024 / in revised form: 15 October 2024 / Accepted: 11 November 2024
© The Author(s) 2024

Abstract Light alloys are being increasingly investigated as alternatives to ferrous-based engineering components, based on weight considerations. However, in-service applications of such light alloy components often require a surface modification step to enhance their wear and corrosion responses for improved functionality. Thermally sprayed cermet coatings offer an enhanced resistance to wear and corrosion. This work investigates WC-CoCr coatings deposited using two different feedstocks comprising fine and coarse powder size distributions on aluminum alloy and steel substrates using high-velocity air-fuel (HVAF) and high-velocity oxy-fuel (HVOF) spray techniques. The WC-CoCr coatings were HVAF sprayed at various parameters to investigate the relationship between the processing conditions, microstructure, and performance. Microindentation, dry sliding wear, dry sand abrasion, cavitation erosion, and corrosion tests were conducted to assess the performance of the coatings. Despite the qualitative similarities in the microstructures of the coatings, the measured microindentation hardness values were observed to vary, and coatings deposited with higher particle impact velocities showed the highest microhardness between 1400 and 1600 HV0.3. For the three categories of wear investigated, the HVAF coatings showed better resistance than the HVOF coating investigated in this study. The estimated average specific wear rate (SWR) due to sliding wear of the HVOF coating was $\sim 16.7 \pm 4.0 \times 10^{-8}$ mm^3/Nm compared to that of the most resistant HVAF coating, which exhibited a SWR of $\sim 1.7 \pm 0.6 \times 10^{-8}$ mm^3/Nm. The cumulative mass loss rate due to the abrasive wear on the HVOF coating reached $\sim$ 1.11 mg/min compared to $\sim$ 0.76 mg/min of the most abrasion-resistant HVAF coating. All coatings showed similar corrosion resistances under the investigated conditions. The combination of wear and corrosion performance of the respective coatings could provide insight into the coating selection for intended applications.

Keywords cavitation erosion · corrosion · HVOF · HVAF · microstructure · WC-CoCr · wear

This article is an invited paper selected from presentations at the 2024 International Thermal Spray Conference, held April 29–May 1, 2024, in Milan, Italy, and has been expanded from the original presentation. The issue was organized by Giovanni Bolelli, University of Modena and Reggio Emilia (Lead Editor); Fardad Azarmi, North Dakota State University; Sara Bagherifard, Politecnico di Milano; Partha Pratim Bandyopadhyay, Indian Institute of Technology, Kharagpur; Šárka Houdková, University of West Bohemia; Heli Koivuluoto, Tampere University; Yuk-Chiu Lau, General Electric Power (Retired); Hua Li, Ningbo Institute of Materials Technology and Engineering, CAS; Sinan Müftü, Northeastern University; and Filofteia-Laura Toma, Fraunhofer Institute for Material and Beam Technology.

✉ Tunji Adetayo Owoseni
tunji.owoseni@hv.se

[1] University West, Trollhättan, Sweden

[2] Volvo Penta, Gothenburg, Sweden

[3] Tampere University, Tampere, Finland

Introduction

Engineering components subjected to challenging functional applications are susceptible to varying surface damage. In the case of marine components, wear and corrosion (Ref 1) and cavitation erosion (Ref 2) are the dominant damage mechanisms. These conditions that promote premature degradation limit the lifespan of the components, raise the cost of doing business, and undermine emerging sustainability efforts. Potential solutions to

Published online: 05 December 2024

combat these identified threats include eliminating or reducing the adverse effects of the causative conditions. Metals used in propeller applications in marine environments are susceptible to corrosion attack and cavitation erosion; wear is also likely because the propeller is coupled to a shaft (sliding) or because solid particles carried in high-velocity flow cause abrasion wear (Ref 3). A combination of these conditions creates the possibility of synergistic degradation, which reduces the lifespan of marine components or installations. Consequently, such components can benefit from protective coatings, which can function as the first line of defense and mitigate rapid deterioration.

Thermally sprayed cermet coatings offer excellent protection against wear and corrosion (Ref 4). Among cermets, WC-CoCr is the most promising candidate material, and high-velocity deposition methods such as high-velocity air-fuel (HVAF) and high-velocity oxy-fuel (HVOF) spraying techniques are the typical coating methods of choice. While high-velocity-based thermal spray techniques (HVOF and HVAF) create dense coatings (Ref 5–7), the spray conditions (Ref 8, 9) and particle size distribution of the feedstock (Ref 4, 9-11) play a key role in governing the microstructure and coating performance against wear or corrosive environments.

Marine propellers are often made of steel, aluminum alloys, or bronze for various sustainability considerations related to installation and maintenance costs (Ref 12-15). The propeller assembly consisted of a shaft, hub, and propeller blade. The shaft is often made of steel, while the hub and propeller blades can be made of either bronze or aluminum alloy. While the shaft and hub are mostly prone to wear (sliding and abrasion), the propeller blade is prone to wear due to sliding, abrasion, and cavitation erosion. Therefore, it is pertinent to study WC-CoCr coatings deposited on steel and aluminum alloy substrates that can provide insights into the wear performance of coated shafts carrying an aluminum propeller subjected to high fluid flow in a solid-particle-prone corrosive liquid. HVOF-sprayed WC-CoCr on stainless steel (Ref 10, 16, 17) and aluminum alloys (Ref 4, 18) have been investigated for wear (sliding and abrasion) and corrosion protection. The effect of substrates (steel, aluminum, and Inconel 625) on the deposition rate and wear performance of HVAF-sprayed WC-CoCr coatings has also been investigated (Ref 19). Similarly, other light alloys (Mg-based) coated with cermets using HVOF have been investigated for their wear and corrosion resistance (Ref 20, 21). However, the implication of varied powder feedstocks deposited on aluminum substrates under different HVAF spray conditions on the ability of a coating to offer combined protection against wear (sliding and abrasion), corrosion, and cavitation erosion has not been comprehensively investigated. This study aims to examine HVAF-sprayed WC-CoCr coatings deposited under varied spray conditions and two distinct particle cut-size feedstocks on steel and aluminum alloy substrates. The coatings deposited on steel substrates were evaluated only for sliding wear, while coatings deposited on aluminum alloy substrates were evaluated for abrasive, sliding wear, cavitation-erosion, and corrosion resistance. The implication of the coating thickness was also investigated for sliding wear protection on steel and aluminum alloy substrates. The outcome of this study is expected to provide valuable insights to assist in deploying the investigated coatings for marine propeller applications.

Materials and Methodology

Coating Preparation

Three different agglomerated and sintered WC-CoCr (86-10-4 mass fraction in %) cermet powder feedstocks were used in the present study: WOKA 3654 (30/10 µm), WOKA 3652 (45/15 µm), and WOKA 3661 FC (20/5 µm), all supplied by Oerlikon Metco Europe GmbH. The coarsest of the three powders, WOKA 3652, was deposited using a propane-fueled DJ2700 high-velocity oxy-fuel (HVOF) torch at the Thermal Spraying Engineering (TSE) facility in Malmo, Sweden. The remaining two powders, WOKA 3654 and WOKA 3661 FC, were deposited by a high-velocity air-fuel (HVAF) spray process using M3 and M2 torches (UniqueCoat, Richmond, USA) at the University West, Sweden. Two M3 nozzles (4L2 and 5L4) were used to process WOKA 3654 under different spraying conditions. Similarly, two M2 nozzles (3L0F and 3L3F)

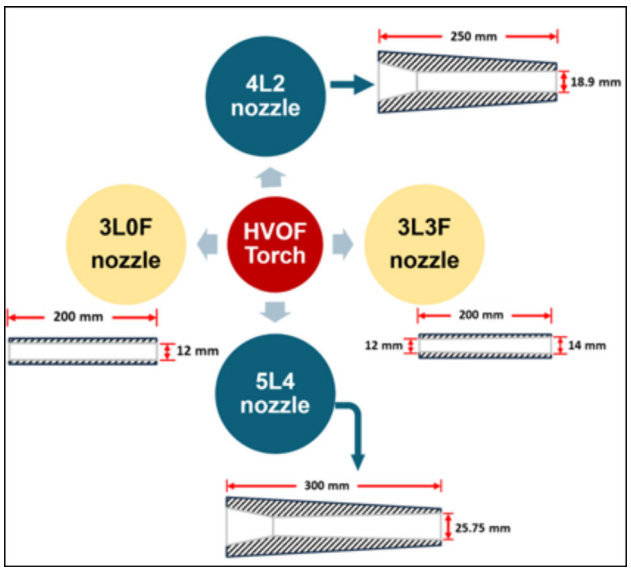


Fig. 1 HVAF spray nozzle configurations and schematics

were used to process WOKA 3661FC powder (see Figure 1). Each M2 nozzle was used to deposit one thin and one thick coating, respectively. The deposition parameters used in the HVAF process are listed in Table 1. The HVAF-sprayed coating samples were marked "AF-1" to "AF-6" to differentiate the varied spray conditions shown in Table 1.

The substrates used for the coating deposition were either coupons or plates. The coupons have a dimension of 25 mm diameter and 6 mm thickness and were made of low-carbon steel SSAB Domex ® 350LA and aluminum alloy ALU 5754—the nomenclatures of coatings deposited on steel coupons were suffixed with "st," while the aluminum alloy coupons were suffixed with "al." The coated coupons were used for coating characterization and dry sliding wear tests. The plate substrates were made of ALU 5754 alloy. The plates had three different dimensions, based on the intended experimental tests that were subsequently performed. The coated plates were used for dry-sand abrasion wear, cavitation erosion, and corrosion testing. The plates used as substrates for abrasion testing of coatings had dimensions of 50 mm × 25 mm × 6 mm, those used for the cavitation erosion tests had dimensions of 25 mm × 25 mm × 6 mm, and those used for the corrosion tests had dimensions of 50 mm × 50 mm × 6 mm with five Ø 5 mm drilled holes. The drilled holes were used to create galvanic contact points and for sample holding during the corrosion test. The drilled holes were then covered during the coating deposition process.

Table 1 HVAF deposition parameters

Parameters	Sample ID					
	AF-1	AF-2	AF-3	AF-4	AF-5	AF-6
Nozzle	4L2	5L4	3L0F	3L3F	3L0F	3L3F
Chamber/Powder	M3/WOKA 3654			M2/WOKA 3661FC		
Injector	3 L	3 L	3 L	3 L	3 L	3 L
Air Pressure (PSI)	106	108	95	95	95	95
Fuel Pressure I (PSI)	100	100	93	93	93	93
Fuel Pressure II (PSI)	105	115	X	X	X	X
Carrier gas (l/min)	40	40	40	40	40	40
Feed (g/min)	200	200	160	180	200	200
SoD (mm)	300	300	200	200	200	200
Surface Speed (m/min)	100	100	100	100	100	100
Step (mm/rev)	5	5	5	5	5	5
Passes	9	12	3	4	9	14

Characterization

The as-received powders WOKA 3654 and WOKA 3661 FC were characterized using scanning electron microscopy to show the powder particle morphology using a tabletop SEM (TM3000, HITACHI, Japan) operated at 15 kV. Sprinkles of individual powders were collected on carbon tapes and gold-coated before low- and high-magnification micrographs were obtained. Low-magnification images were used to analyze the particle size distribution (PSD) using image analysis with a Java-based software called ImageJ (Image J 1.53e, Fiji), freely available in the public domain. A cross section of the feedstock powder was obtained by SEM imaging of hot-mounted particles in resin, polished, and gold-coated. Energy-dispersive x-ray spectroscopy (EDX) (Oxford Instruments, UK) attached to the tabletop SEM was used for elemental mapping of the as-received powders, as-deposited coatings, and tested coating wear tracks.

The cross sections of the coatings were examined using standard metallographic procedures. The porosity of the coatings was determined using image analysis with ImageJ software. Since the analysis was performed primarily to assess the role of spray conditions, samples AF-3 and AF-4 were excluded from the porosity measurements because they were thinner versions of AF-5 and AF-6, respectively, spayed with identical spray parameters. The microhardness of the coatings was measured on the coating cross sections using a Vickers hardness (HV) tester (Duramin-40, Struers, Germany). A normal load of 300 gf was applied to the polished cross section of the samples for a dwell time of 10 s. Ten indents were made per coating to report the average Vickers hardness (HV) with the associated standard deviation.

Wear Tests

Dry Sliding Wear

Dry sliding wear tests were performed on the coatings sprayed on both steel and aluminum alloy substrates using a tribometer (TRB3, Anton Paar, Netherlands) based on the ASTM G99 standard (Ref 22). The wear-test configuration was a ball-on-disk setup under ambient conditions. The wear tests were conducted using an alumina ball of 6 mm diameter as a counter-body with 20 N load at a speed of 0.2 m/s for a 5000 m sliding distance and a track radius of 7 mm. The wear test was repeated for the stated parameters on the same sample at a track radius of 9 mm. Before testing, the coated coupons were polished to a surface roughness of < 0.2 µm and cleaned with ethanol in an ultrasonic bath to remove any surface debris due to the polishing procedure. The specific wear rate (SWR) of the

coatings was calculated based on two wear tracks per tested coupon. The SWR was calculated based on Archard's equation, as given in Eq 1.

$$\text{SWR} = V / (F\,x\,d) \quad \text{(Eq 1)}$$

Here, F denotes the normal load applied in 'N,' d is the sliding distance in 'm' and V represents the total volume loss of the wear track in 'mm^3.' The volume loss of the wear track was calculated from the product of the average of four cross-sectional areas across the worn surface and the circumference of the circular profile of the wear track. The cross-sectional area of the wear track was measured using white light interferometry (WLI), a non-contact surface profilometry technique, using Profilm 3D (Filmetrics Europe GmbH, Germany).

Dry Sand Abrasion Wear

The coated rectangular aluminum alloy plate (50 × 25 × 6 mm) samples were subjected to dry sand-rubber wheel abrasion tests using an abrasion rig (abrasion tester, DUCOM, India) based on the ASTM G-65 standard (Ref 23). The tests were conducted on the as-sprayed samples using a SiO_2 quartz-based abradant medium with a particle size distribution corresponding to AFS 66 (Quarzwerke, Germany). The test was performed at a normal force of 130 N applied on the back of the substrate to press the coating top surface against a rubber wheel (227 mm diameter and 13 mm width rotating at a speed of 200 rev/min), while the abradant flowed between the coating surface and the rubber wheel at a feed rate of 300-400 g/min. The HVOF-sprayed samples were tested twice to confirm the repeatability of the test. Thereafter, each of the HVAF-sprayed samples was tested once; in all cases, the total test duration for each sample was 40 min, with the samples being weighed at 10-minute time intervals. Mass loss due to abrasion wear was determined by weighing the samples before and after each test using a laboratory weighing scale (PCE Deutschland GmbH) with a precision of ± 0.1 mg. The average values of the mass difference and the associated standard deviation for each test duration were plotted against the test duration in minutes for all coatings.

Cavitation Erosion

The cavitation erosion resistance of the HVOF and respective HVAF coatings was investigated using the alternative indirect test method described in the ASTM G32 standard. The experimental setup used a vibratory apparatus based on ASTM G32 parameters. Each test sample (25 × 25 × 5 mm^3) was mirror polished using standard metallographic procedures. Each weighed sample was attached to a sample holder, and the tip of the test equipment was lowered to 0.5 mm distance into the test bath. Each sample was cleaned with ethanol in an ultrasonic bath, dried, and weighed before and after each 1 h test cycle. For each cycle, the sample was kept stationary and submerged in deionized water, while the tip vibrated at a frequency of 20 kHz and an amplitude of 50 µm. Each coating was tested for 6 h. The maximum erosion rate for each tested sample was estimated from linear curve fitting of the measured cumulative weight loss. Volume losses were calculated using a material density of 13.93 g/cm^3 for WC-10Co4Cr. (Ref 24). The average thickness loss and maximum erosion rate (µm/h) of each tested coating were obtained by dividing the volume loss by the tip area of 188 mm^2. The test procedure was performed only once for each test specimen because of the relatively long test duration and good repeatability typically observed in this test.

Corrosion

The corrosion test was set up to initiate galvanic corrosion at one of the Ø 5 mm drilled holes on the coated plate. A copper washer was locked down in direct contact with the WC-CoCr coating with a stainless steel screw at the Ø 5 mm drilled hole. The washer/screw combination was masked with tape before the plate was painted. The painting had two steps: an Axalta alesta EP primer was first applied, followed by an alesta E topcoat. After the paint was allowed to dry, part of the painted plate was exposed by scribing a line through the coating using a diamond cutting disk. The scribed line allowed the corrosion media to reach the paint–coating interface and the coating–substrate interfaces. The corrosion testing was performed in a ControlArt machine type 2 climate test chamber at the Volvo Penta Marine Test Centre using a bespoke experimental marine test cycle—a seven-day cycle with varying temperature and humidity (see Table 2). Three samples for each of the HVOF and the HVAF coatings were tested simultaneously, and the corrosion test lasted for a 16-week duration. The impact of the corrosive environment on the test samples was investigated using electron microscopy

Table 2 Simulated marine atmosphere parameters

S/N	Parameters	Specifications
1.	Temperature	30–45 °C
2.	Relative Humidity	55–95%
3.	Mist—synthetic seawater with 5 % salinity (BS211 part 2.1 kb)	30 min, three times
4.	Rain—deionized water and 5 % NaCl	45 min, two times

and EDX analysis. One sample from each of the test specimens was sectioned through the washer/screw setup to examine the stacked interfaces and possible galvanic activities.

Results and Discussion

Microstructure

As-Received Powder

The characteristics of the as-received cermet feedstock powders are shown in the scanning electron micrographs and particle distribution plots in Fig. 2. The finer of the two feedstocks (WOKA 3661 FC) is presented in Fig. 2(a) and (b), whereas the coarse-cut (WOKA 3654) is shown in Fig. 2(c) and (d). The particle morphologies of both feedstocks shown in Fig. 2(a) and (c) are mostly spherical, although the powder also contains some angular-shaped particles. The surfaces of the individual particles show randomly distributed pores. The polished cross section of the powder particle shown in Fig. 3 was obtained from a sample taken from the coarse powder (WOKA 3654) and prepared as described in Section "Characterization." Only one of the powders was used for this cross-sectional analysis to ascertain the typical morphology and the accompanying elemental distribution because all three powders have the same specifications, except for the variations in size distribution. A representative cross-sectional view of the powder particles shown in Fig. 3 shows a spherical morphology as was seen in the earlier presented free-standing particles—this is consistent with the powder manufacturing route of agglomeration and sintering. The internal features showed areas of distributed pores and binder accumulation. The accompanying EDX analysis of the particle in Fig. 3 shows the elemental composition of the feedstock and the respective quantities of the elements. The quantity of the elemental composition compared to the specifications of the manufacturer matched with the WC at 85.6 wt. % and CoCr binder adding up to 14.4 wt. %.

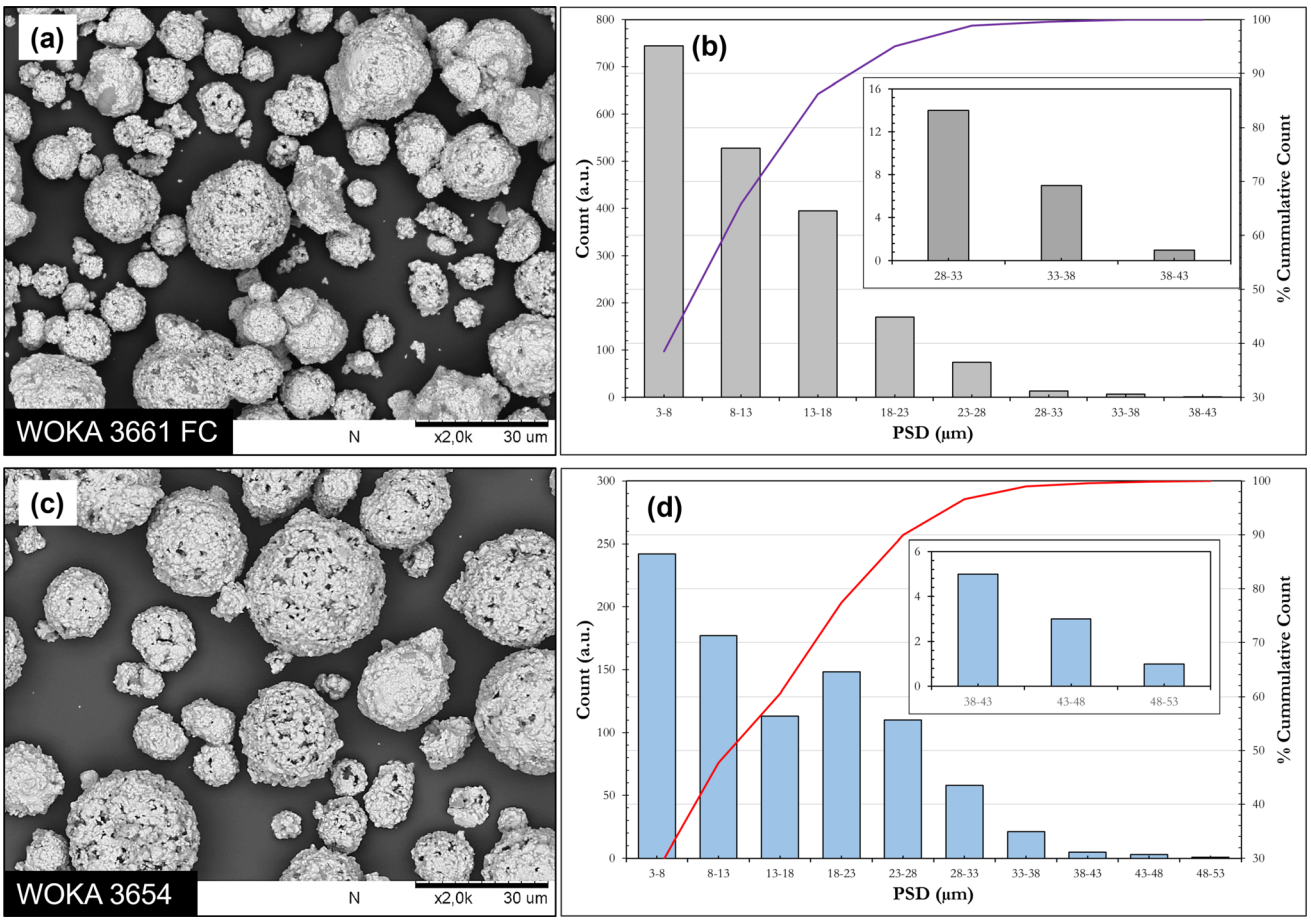


Fig. 2 Morphology of the as-received WC-CoCr feedstock and the estimated particle size number distribution plots: fine-cut in (a) and (b); coarse-cut in (c) and (d)

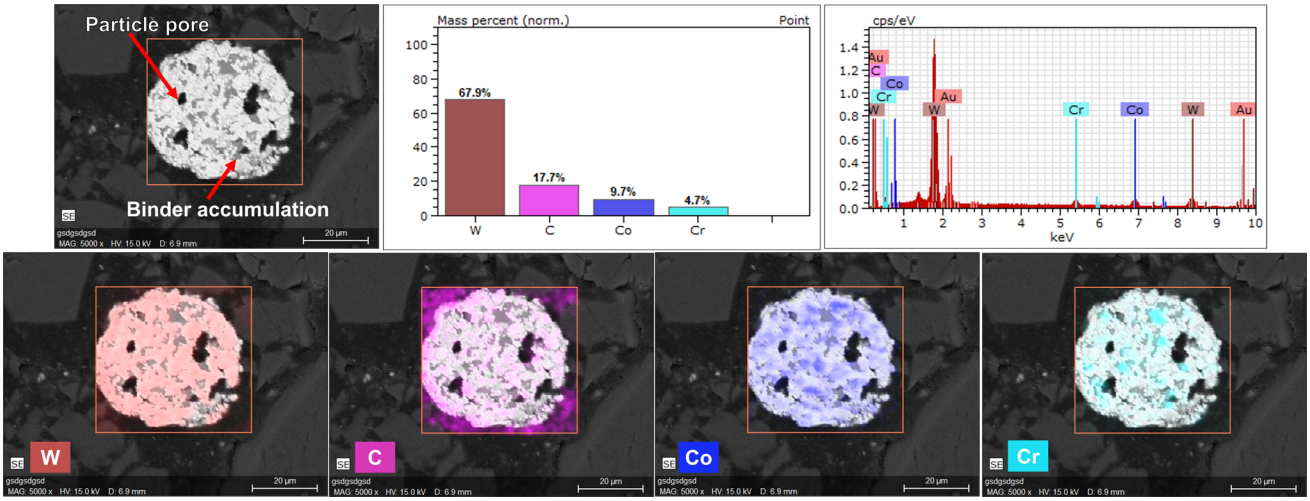


Fig. 3 Cross-sectional morphology of the feedstock particle showing the binder material and particle pores

Table 3 Elemental wt. % composition of coatings

Elements	HVOF	AF-1	AF-2	AF-5	AF-6
W	74.67	75.84	76.70	75.72	76.48
C	8.73	7.43	7.91	8.23	8.67
Co	12.14	11.93	10.96	11.48	10.51
Cr	4.46	4.80	4.42	4.58	4.34
WC	83.40	83.28	84.62	83.94	85.15
CoCr	16.60	16.73	15.38	16.06	14.85
Total	100.00	100.00	100.00	100.00	100.00

Table 4 Porosity (%) of WC-CoCr coatings

Porosity (%)		HVOF	AF-1	AF-2	AF-5	AF-6
	Average	0.7	2.4	1.6	1.0	1.5
	St. Dev.	0.6	0.8	0.6	0.1	0.2

As-Sprayed Coatings

The coatings deposited in this study used two distinct processing techniques (HVOF and HVAF) and substrate materials (SS and Al). The elemental compositions of the coatings, as determined from EDX shown in Table 3, suggest that all the coatings, irrespective of the processing technique or the feedstock, show a WC content of $\sim 84.08 \pm 0.8$ wt. % and a CoCr content of 15.92 ± 0.8 wt. %. The results indicated no significant elemental variations between the coating samples and the feedstock. Given that both HVOF and HVAF are very high-velocity techniques that involve low residence times of the powder particles in the flame, significant elemental depletion was neither expected nor observed. Previous studies have shown that some degree of decarburization can indeed occur in the case of HVOF owing to the relatively higher temperature exposure of WC particles compared with HVAF (Ref 4, 25). However, the corresponding changes in the carbon and oxygen contents were too small to be reliably captured by the EDX analysis.

In addition to the elemental composition of the coatings, the deposition conditions adopted during thermal spraying also influence the microstructure of the coatings (such as the porosity content), which in turn influences the coating properties and performance (Ref 10, 26). The measured porosities of the coatings, based on the deposition conditions, are listed in Table 4. Given the porosity measurement approach described in the subsection on coating characterization above, it is relevant to note that distinguishing between segregated binders and actual porosity based on grayscale is extremely challenging. Notwithstanding the above, the measured porosities of the coatings were approximately 2% or less in all cases. Given the low porosity values and the uncertainty associated with the measurement, as reflected in the standard deviation values, it is inappropriate to correlate the porosity values with the microhardness, observed specific wear rate (SWR), and corrosion data to be presented in subsequent subsections.

The characteristics of the feedstock (Ref 27, 28) and the properties of the substrate (Ref 20, 21) could also influence the build-up of thermal spray coating. Practically, the first few splats impacting the substrate create varying morphologies based on the deposition angle and particle impact

energy. The substrate influences splat formation only during the early stages of coating formation (the first couple of layers), after which there is no significant substrate effect, as shown in a previous study by this group. (Ref 19). As such, the overall microstructure of the various individual coatings deposited in this study is not expected to vary because of the substrate materials, irrespective of the spray deposition technique—either HVOF or HVAF. Therefore, only the microstructures of coatings deposited on aluminum substrates have been shown to compare the microstructures of the respective coatings deposited using varying spray conditions and powder feedstocks. The coating deposited by the HVOF technique and the two coatings sprayed with the coarse-cut feedstock marked AF-1 and AF-2 are shown in Fig. 4. The cross sections of the coatings show a good coating–substrate interface. The magnified views of the coatings shown in Fig. 4 (b), (d), and (f) reveal no obvious defects. The three coatings showed a homogenous distribution of the CoCr binder matrix, with no obvious regions of binder accumulation. The coating buildup depends on the extent of the thermal softening of the binder and the overall particle impact energy, which depends on the inflight particle velocity controlled by the spray parameters (Ref 29).

The fine-cut powder feedstock deposited with two different nozzles created four coating samples, AF-3, AF-4, AF-5, and AF-6—the parameters implemented for the four coatings had no secondary fuel inflow, but there is a slight variation in powder feed rate and the number of spray passes for the respective coatings. AF-3 and AF-4 were sprayed to ensure that the coating thickness was not less than 50 μm, whereas those of AF-5 and AF-6 were not to be less than 200 μm. The resulting coating thickness and microstructure based on the spray conditions are shown in Fig. 5, as a measure of the deposition rate. The magnified cross section of the two thin coatings in Fig. 5(b) for AF-3 and Fig. 5(d) for AF-4 showed a defect-free coating–substrate interface with spots of binder accumulation within the coating. Similar observations were made for the magnified micrographs of AF-5 and the AF-6 coatings. The bonding between successive layers during the deposition is facilitated by a combination of high particle impact velocity and particle temperatures in both cases, despite the different spray conditions engendered by the two nozzles.

Microhardness

The indentation on the respective coatings at a monotonous loading of 300 gf (2.94 N) provided the Vickers hardness values of the tested coatings. The microhardness values for all six HVAF coatings and that of the HVOF coating lie in the same standard deviation range from an average of 1250–1550 HV0.3, as shown in Fig. 6. The microhardness of the HVOF coating was $\sim$ 1290 $\pm$ 173 HV0.3, compared to the six HVAF coatings, with average values between 1250 and 1550 HV0.3. Comparing different HVAF coatings, the coatings sprayed from the coarse powder (AF-1 and AF-2) using the M3 nozzle showed average microhardness values between 1300 and 1450 HV0.3, as compared to the coatings sprayed from the fine-cut powder (AF-3–AF-6) using the M2 nozzle, whose average microhardness matched the overall range for the HVAF coatings (1250-1550 HV0.3). The top three average values were for HVAF coatings deposited under spray conditions that engender a high particle impact velocity—5L4 in the case of AF-2 and 3L3F for AF-4 and AF-6.

Wear Behavior

Dry Sliding Wear

The sliding wear performance test based on the test parameters presented in Section "Dry Sliding Wear" shows a clear distinction in the performance of the HVAF coatings relative to the HVOF sample. The performance of the respective coatings provides insight into their wear resistance for a choice relevant to the intended marine application. The observed wear performances of the samples presented in Fig. 7 show disparity based on the processing techniques, spray parameters, coating thickness, and choice of substrate.

Effect of the Spray Process

Based on the processing techniques, the HVAF coating SWRs were lower than those of the HVOF samples, irrespective of the substrate used. The only outlier was AF-3 on an aluminum substrate—it showed the highest SWR among all samples. The higher deposition temperature in HVOF coatings causes the binder materials in the feedstock particles to be softened or molten, leading to a reduced impact velocity when compared to HVAF (Ref 30, 31). The softened particles traveling at supersonic speed mean that the impact energy is mostly dissipated in spreading the particles rather than creating a peening effect at the impact point. As such, the bonding created by the impinging particles' kinetic energy may not have been sufficient to resist the repeated shear created by the sliding wear condition; hence, its SWR was higher than that of the HVAF coatings.

Effect of HVAF Spray Parameters

The performance of the respective coatings depends on the microstructure of the coatings built based on the characteristics of the spray particles (temperature and velocity)

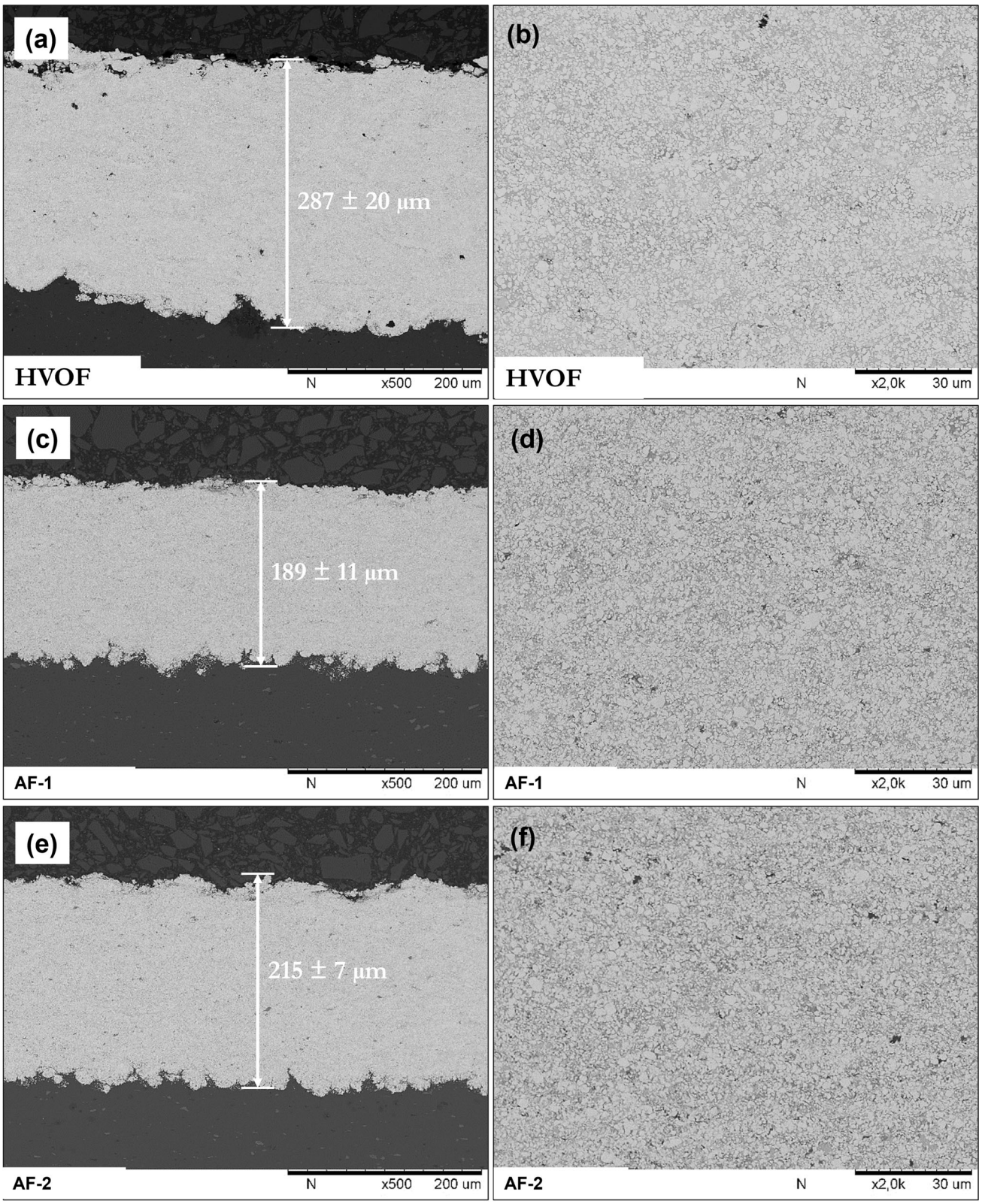


Fig. 4 Cross-sectional micrographs at low and high magnifications of the HVOF coating and the HVAF coatings deposited with the coarse-cut powder: HVOF samples in (a) and (b), AF-1 samples in (c) and (d) and AF-2 samples in (e) and (f), respectively

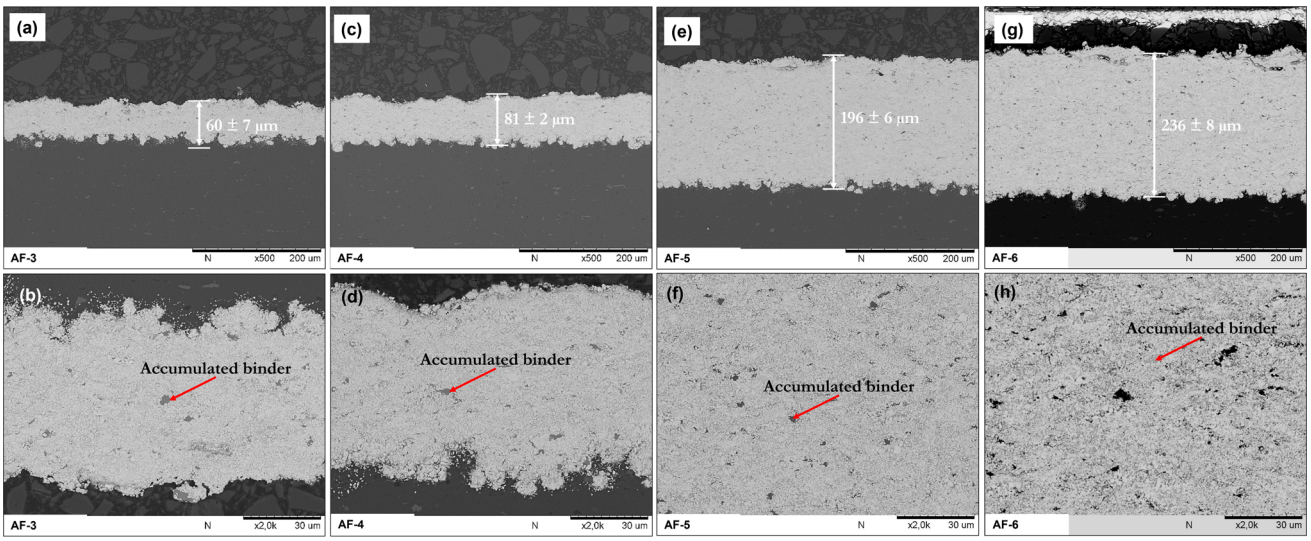


Fig. 5 Cross-sectional micrographs of the HVAF coatings deposited with the fine-cut powder showing the thin coatings AF-3 and AF-4 in (a)–(d) and the thick coatings AF-5 and AF-6 in (e)–(h), respectively

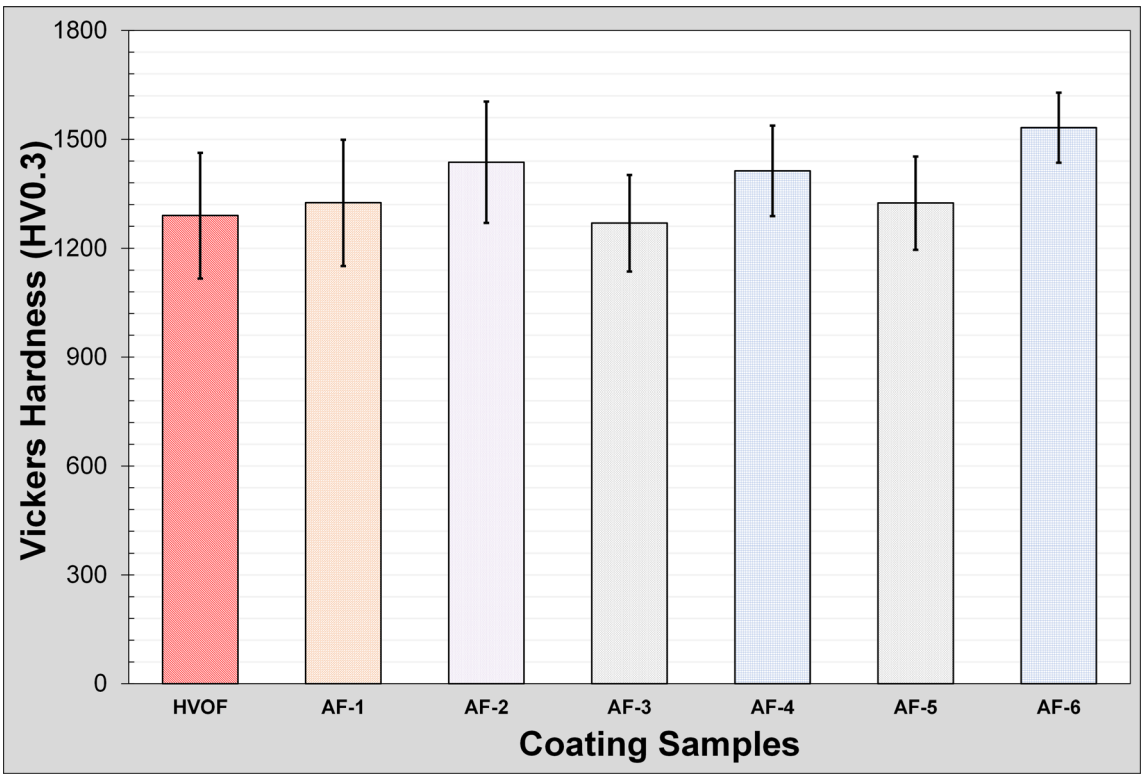


Fig. 6 Vickers microhardness of the HVOF and the HVAF coatings measured at 300 gf

engendered by the feedstock's physical properties and spray conditions. Of the four nozzles used to deposit the HVAF coatings, the 4L2 and 3L0 nozzles engender higher particle heating and lower impact velocity compared to the 5L4 and 3L3F nozzles, which will have a higher impact velocity. A high impact velocity causes an increased peening effect, which leads to improved interparticle cohesion in the coating layers. Therefore, the two coatings

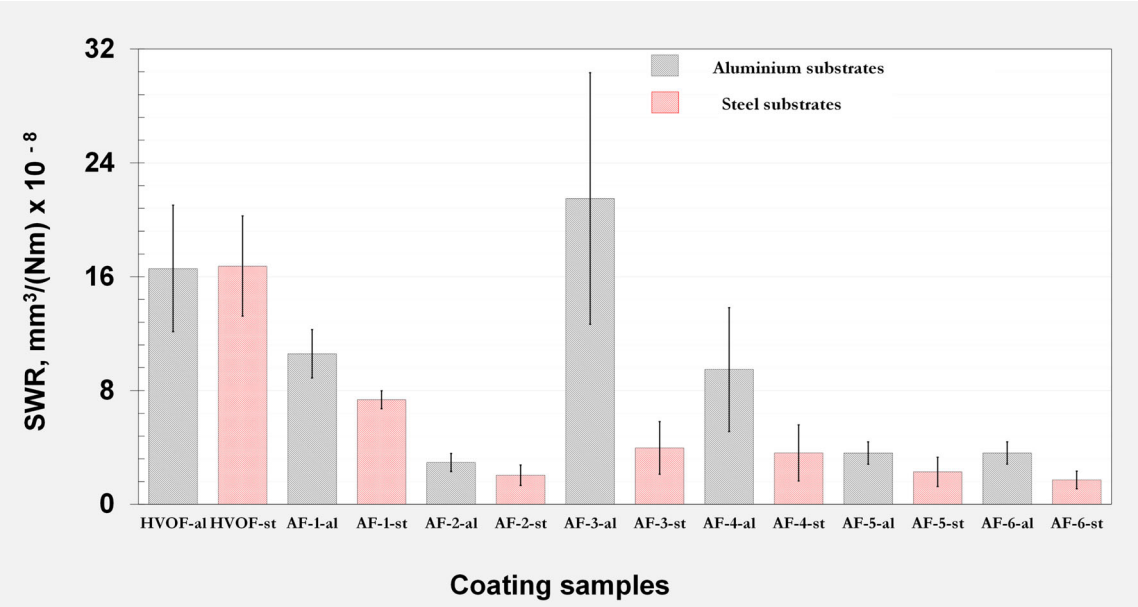


Fig. 7 The specific wear rates (SWR) of the tested WC-CoCr coatings were compared based on the deposition techniques and choice of substrates, and the SWR for coatings on an aluminum substrate was plotted side by side with those deposited on a steel substrate

deposited with the 5L4 and 3L3F nozzles, AF-2 and AF-6, benefited from the peening effect created by the deposition conditions used to reduce the average SWR for coarse and fine-cut feedstocks. The AF-2 sample also on account of the superior impact velocity enabled by the 5L4 nozzle and being a thicker coating with repeated impact of the particles that build the adjoining layers demonstrated the least SWR.

Effect of Coating Thickness and Substrate Material

Independent consideration of the SWR of the HVAF coatings provides insight into the role of the spray conditions on the respective coatings vis-à-vis the feedstock and substrates used. The effect of substrate material in HVAF spraying of WC-CoCr on coating formation mechanisms and wear performance has been extensively studied in previous work, showing that the substrate material has a significant influence on coating formation (Ref 19). The aluminum substrate with lower hardness and yield strength resulted in extensive plastic deformation of the substrate and penetration of particles into the substrate, while deposition on the steel substrate resulted in the kinetic energy of the accelerated feedstock being utilized to produce deformed splats. However, the thick coatings showed similar overall microstructures and wear resistances, indicating that the substrate played a minor role in the evaluation of the thick coatings. This was attributed to the initial influence of the substrate becoming insignificant when subsequent layers were sprayed on a surface with the same material and characteristics (Ref 19). Similar wear performance was also observed in this work, both in the case of thick coatings deposited by HVAF and HVOF, when comparing coatings on steel and aluminum substrates.

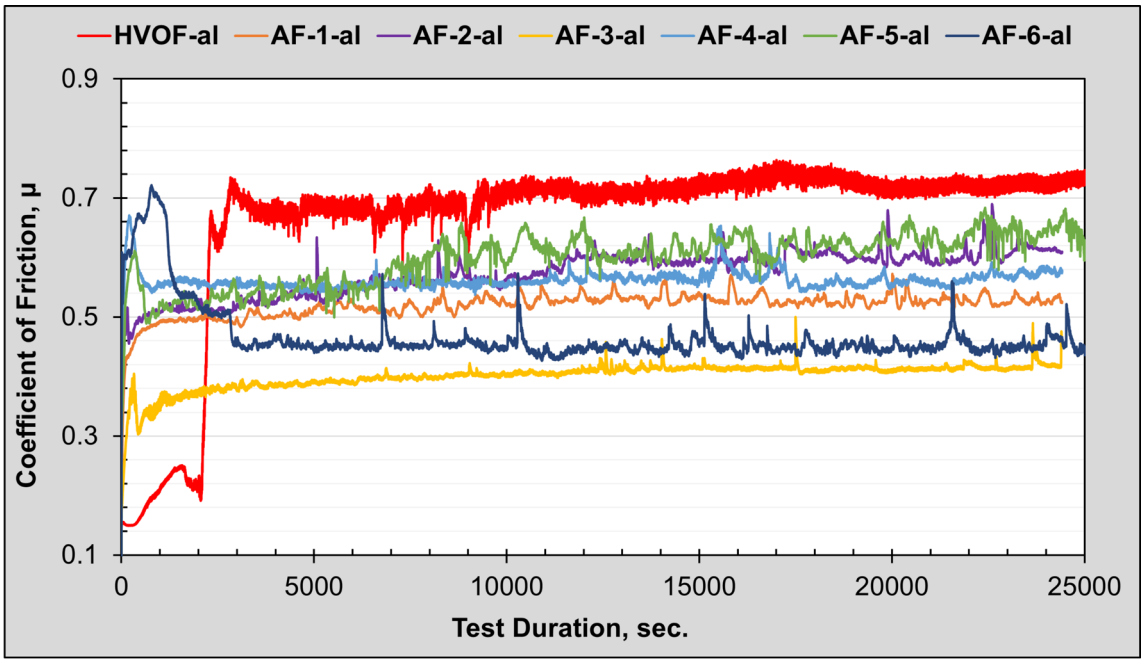
The effect of coating thickness on the wear performance of the WC-CoCr coatings has been also investigated earlier. It has been shown in previous work that for HVAF-sprayed WC-CoCr coatings on steel substrates, at a sliding wear test load of 20 N, the SWR increased by two to three times for a coating thickness of 100 µm or less as compared to thicker coatings, which was attributed to the transfer of the test load to the underlying substrate (Ref 32). This difference was less pronounced when the wear tests were performed at a lower load of 10 N and were not significant at a test load of 5 N. A similar effect of coating thickness on the wear performance of HVOF-sprayed WC-CoCr on aluminum substrates was observed by Bolelli et al., however, at a lower sliding wear test load of 10 N (Ref 18). Comparing these two studies, the reason this influence was observed at a lower test load could be attributed to the lower hardness and yield strength of the aluminum substrate, suggesting a higher transfer of the test load to the substrate than in the case of steel.

This phenomenon can also be observed in this work, where the thin coatings showed a higher SWR than the thick coatings. The difference was more pronounced in

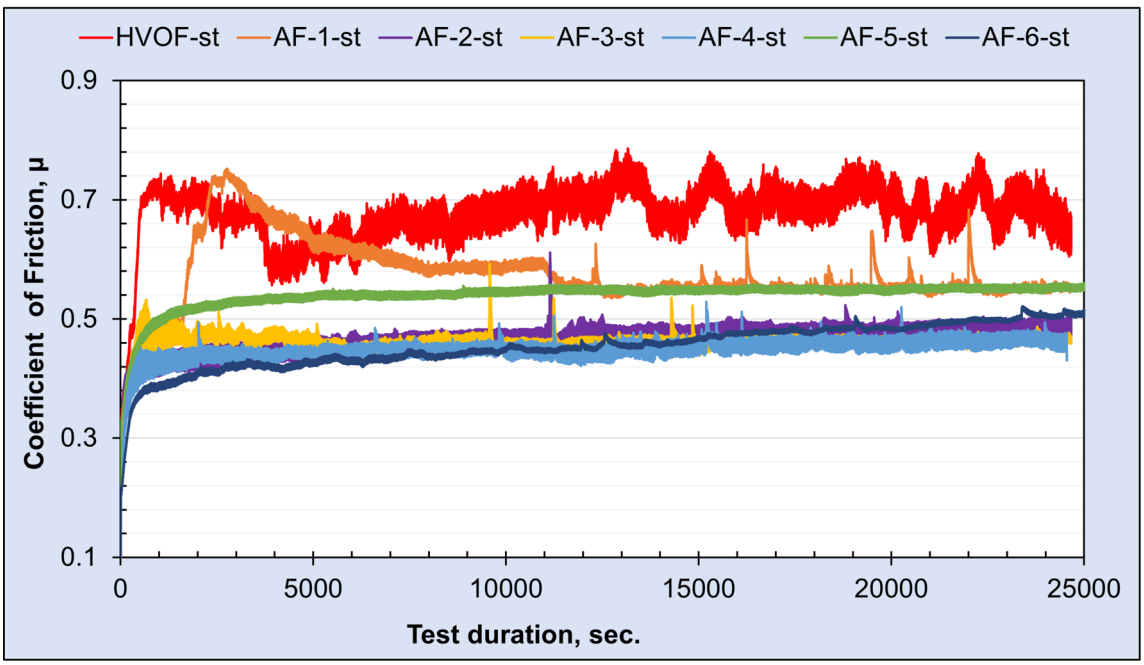
the case of the aluminum substrate, comparing AF3 versus AF5 and AF4 versus AF6, concurring with the discussion above. The reason for the higher variation between the substrates in the SWR of AF-3 than AF-4 could be explained by the lower coating thickness of AF-3, where the coating thickness can play a more significant role.

CoF Results

The sliding contacts between each of the respective coatings and alumina counter body were reflected in the recorded coefficient of friction (CoF) values from the respective tests (Fig. 8). The CoFs recorded for the tests on



(a)



(b)

Fig. 8 Variation of coefficient of friction (CoF) against test duration for HVOF and HVAF-sprayed WC-CoCr coatings (a) on aluminum alloy substrate (b) low carbon steel substrate

the samples sprayed onto the aluminum substrate are shown in Fig. 8(a), whereas those for the samples on the steel substrate are shown in Fig. 8(b). In both cases, the average steady-state value of the CoF for the HVOF sample averages 0.7 while for the HVAF samples the average lies between 0.4 and 0.55. Overall, the sliding contacts showed a short run-in period that lasted for ~ 500 s, except for the HVOF-sprayed sample on the aluminum substrate that reached ~ 2500 s.

Wear Tracks

Microstructural analysis of the wear tracks of the tested samples was performed using scanning electron microscopy aided by EDX for elemental mapping. The microstructural study of the wear tracks reflects the notable distinction between the HVOF and the HVAF coatings. In both cases, there are proofs of material transfer (see Fig. 9 and 10), while the HVOF coating, in addition to the transferred material, also shows wear debris (see Fig. 9b). The wear track of the HVOF samples in Fig. 9 is wide (~ 1000 µm) and covered by patches of transferred material. The EDX analysis of the wear tracks showed that the patches and debris contained mostly aluminum and oxygen from the alumina counter body. The presence of the material transferred from the ball and wear debris suggests that there are combined wear mechanisms that explain the increased material removal experienced by the HVOF sample. The patches on the wear track were proof of adhesive wear, whereas the debris substantiated the presence of abrasive wear. The debris generated from the worn alumina balls and the coating surface can be incorporated between the coating surface and the counter body to create a three-body abrasive wear condition that leads to a severe wear regime. In Fig. 10, representative micrographs of the wear tracks of the HVAF coatings are presented: one set of the tested coatings deposited from the coarse powder WOKA 3654 (AF-1) and the other from the fine-cut powder WOKA 3661FC. The wear tracks of the tested samples of the HVAF coatings were similar in terms of the width and transferred material, irrespective of the deposition conditions. The EDX analysis performed on the wear track of a typical HVAF coating is shown in Fig. 11. However, the distribution of the transferred material across the track was sparse compared with that observed on the wear track of the HVOF coatings. There was also no wear debris on the wear track, suggesting that the dominant wear mechanism for most of the HVAF coatings was adhesive wear.

Dry Sand Abrasion Wear

The abrasive wear resistance of the HVAF and HVOF coatings, expressed by mass loss against time, are presented in Fig. 12. The mass loss approach was employed to compare the resistance of the tested coatings because the test conditions created a wider irregular wear track that was difficult to analyze for volume loss using the WLI approach, as was used for the dry sliding wear test samples. Mass loss analysis as a measure of abrasive wear resistance

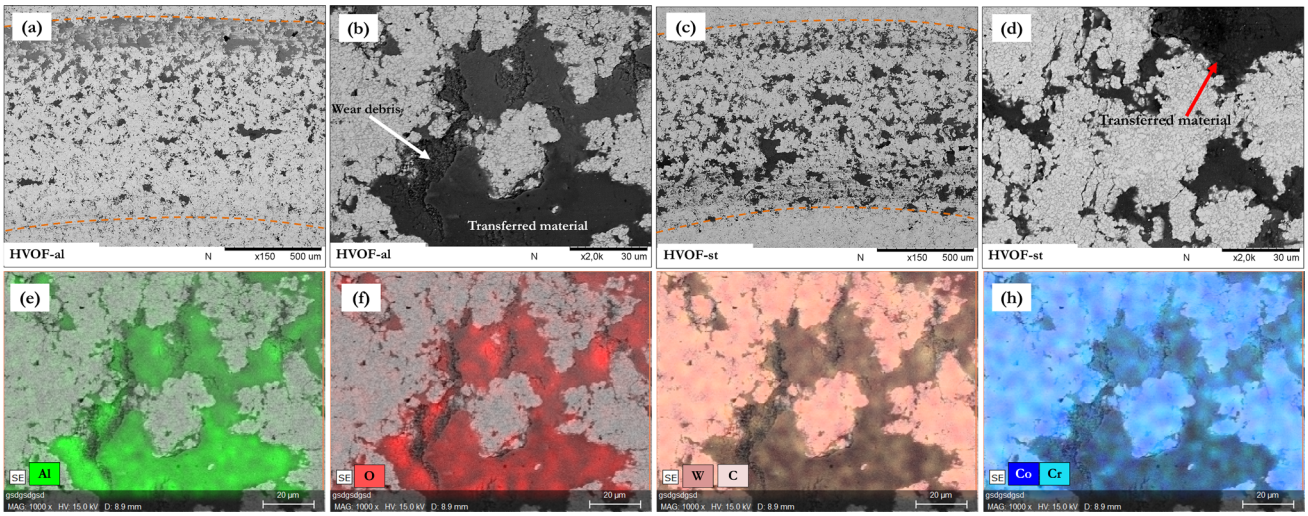


Fig. 9 Scanning electron micrographs of the tested HVOF coating wear tracks (a)–(b) coating on an aluminum substrate (c)–(d) coating on a steel substrate (e)–(h) EDX analysis of the wear track showing the elemental composition of the wear debris and materials on the wear track

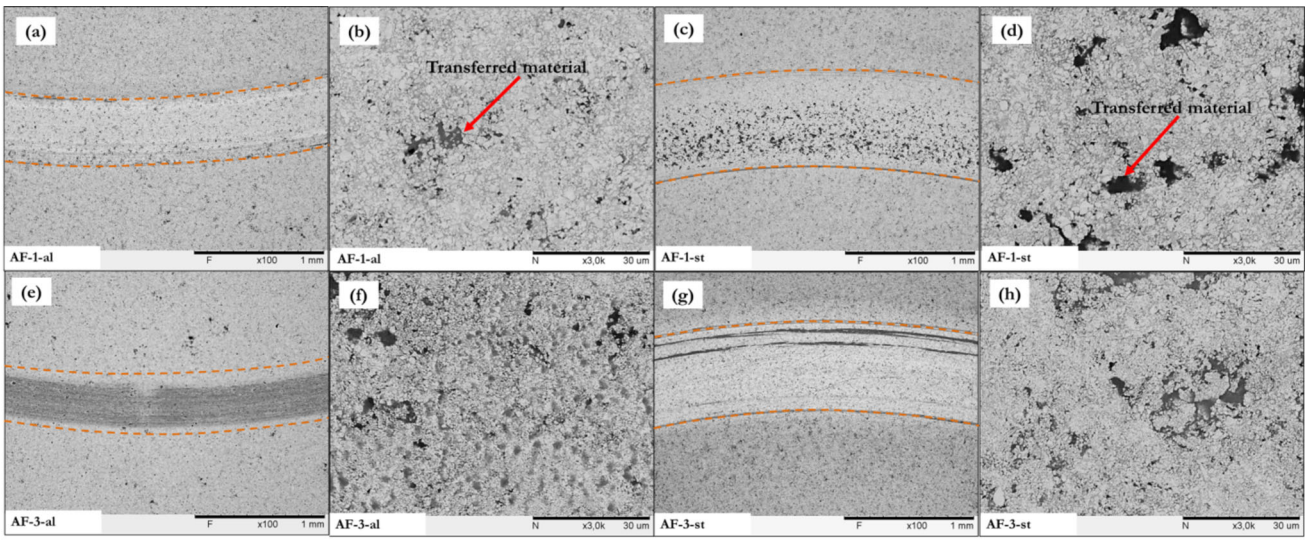


Fig. 10 Scanning electron micrographs of the representative HVAF coating wear tracks showing transferred materials within the tracks (a)–(b) coarse powder deposited on an aluminum substrate (c)–(d) coarse powder deposited on a steel substrate (e)–(f) fine powder deposited on an aluminum substrate (g)–(h) fine powder deposited on a steel substrate

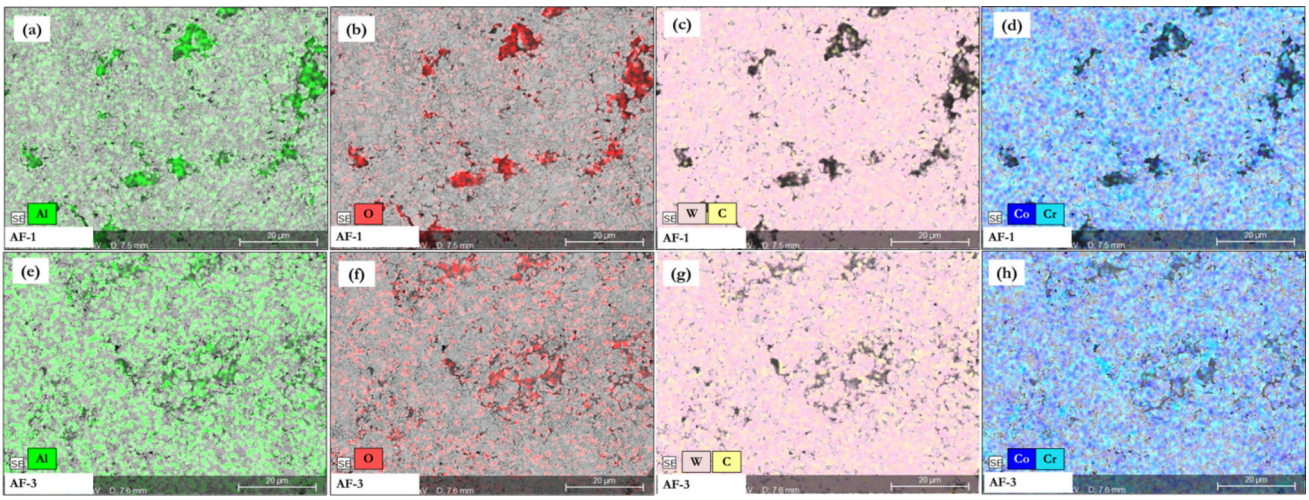


Fig. 11 EDX analysis of the wear tracks of selected HVAF coatings showing the elemental composition of the materials on the wear track (a)–(d) AF-1 coating (e)–(h) AF-3 coating

was employed to compare coatings of the same material and similar microstructures (Ref 33). The two thin coatings (AF-3 and AF-4) failed before the first ten minutes of the abrasion test, as the underlying substrate was exposed. A retrospective test of 5 min was performed on each of them to determine the period in which failure occurred. The results showed that failure occurred beyond 5 min during the test, as the coatings remained intact after the 5-minute test. The results in Fig. 12 show that the remaining four thick HVAF coatings offer improved abrasive wear resistance to varying extents compared with the HVOF coating. Each data point of the HVOF sample is the average of two

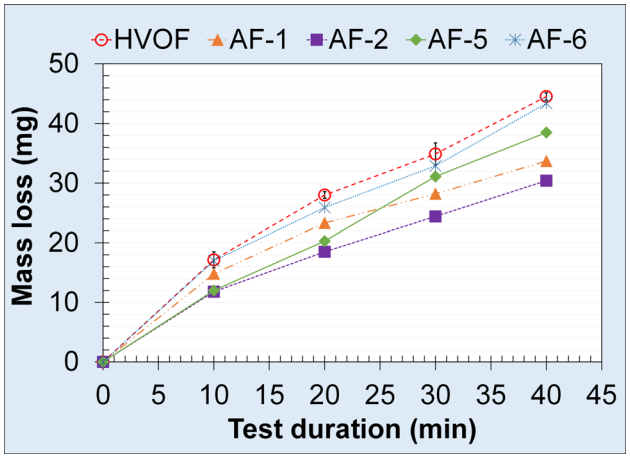


Fig. 12 Combined plots of mass loss against time measured for the HVAF and the HVOF coatings recorded at 10-minute intervals during the dry sand abrasion wear test for a test duration of 40 min. Each data point of the HVOF sample is the average of two tests with the associated standard deviation

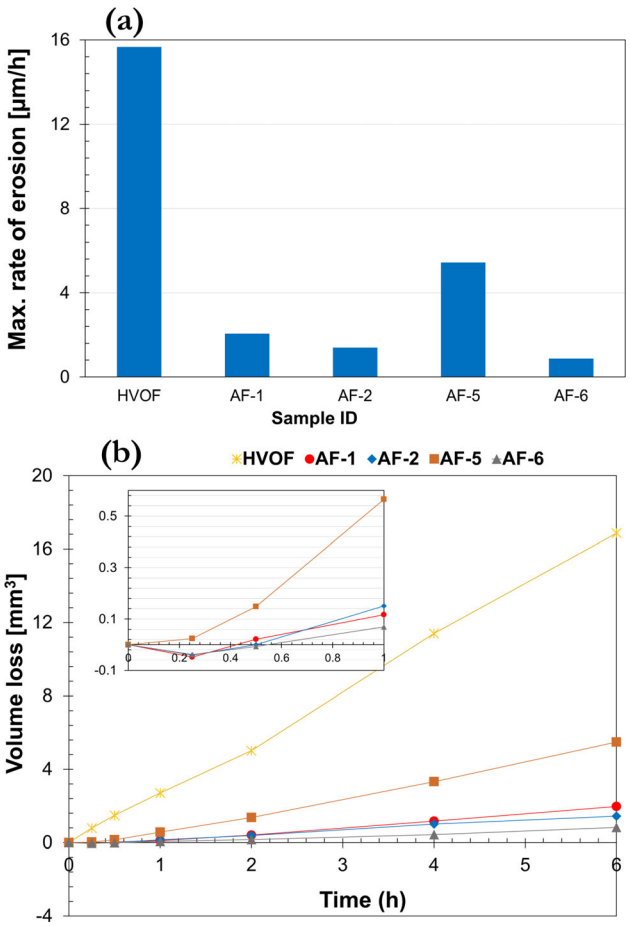


Fig. 13 The cavitation erosion resistance of the HVOF coating and the thick HVAF coatings (a) volume loss (mm^3) against time (h) (b) maximum rate of erosion for each sample

tests with the associated standard deviation. The low standard deviation for the individual data points suggests good repeatability of the test procedure. Of all the coatings, the AF-2 coating showed the best resistance to abradant rubbing against its top surface pressed against a rubber wheel, irrespective of the coating processing techniques. This performance is consistent with the previously described microstructural build of the AF-2 coating engendered by the spray conditions listed in Table 1. However, the coatings deposited from the fine-cut powder feedstock, AF-5 and AF-6, showed more mass loss compared to the two coatings deposited from the coarse powder, AF-1 and AF-2. The performance of the respective coatings indicated the highest slope of mass loss (mg) against time (min) in the first 10 min of the test. This suggests that as soon as the as-deposited top surface roughness became worn to reach a run-in status, the underlying coating layers subsequently interacted with the flowing abradant under similar conditions, causing constant material removal, which established the repeatability of the test conditions. The overall slope of the trend lines of the individual coatings also shows that the AF-1 and the AF-2 coatings have lower values compared to those of the AF-5 and the AF-6 coatings.

Cavitation Erosion

The cavitation erosion performance of the HVOF coating and the thick HVAF coatings sprayed using the coarse- and fine-cut powders were evaluated in terms of volume loss (mm^3) per hour. The results in Fig. 13 show a clear distinction between the coatings sprayed with fine-cut powder and those sprayed with coarse powder. The AF-6 coating sample demonstrated the highest resistance to cavitation erosion. The progression of the cavitation erosion stages is depicted in the plot of volume loss against time, as shown in Fig. 13(b). Cavitation erosion has three stages that are marked by unique features. The initial stage had a near-zero erosion rate compared with the later stages. At this initial stage, the incubation period and submicron-sized pits were created. The following stage is the acceleration period, during which the number and size of the pits increase in addition to the formation of cracks and craters. The final stage is the deceleration period, in which erosion actions are reduced across the solid surface (Ref 34). The volume loss plot in Fig. 13(b) suggests that the AF-6 and HVOF samples had the longest and shortest incubation periods, respectively. The succeeding acceleration period was the fastest in the HVOF sample among all the coatings, considering the volume of material loss per hour, in sharp contrast to AF-6, which showed the lowest volume loss of material per hour.

The mechanism behind the observed cavitation resistance of the five tested coatings can be explained using the

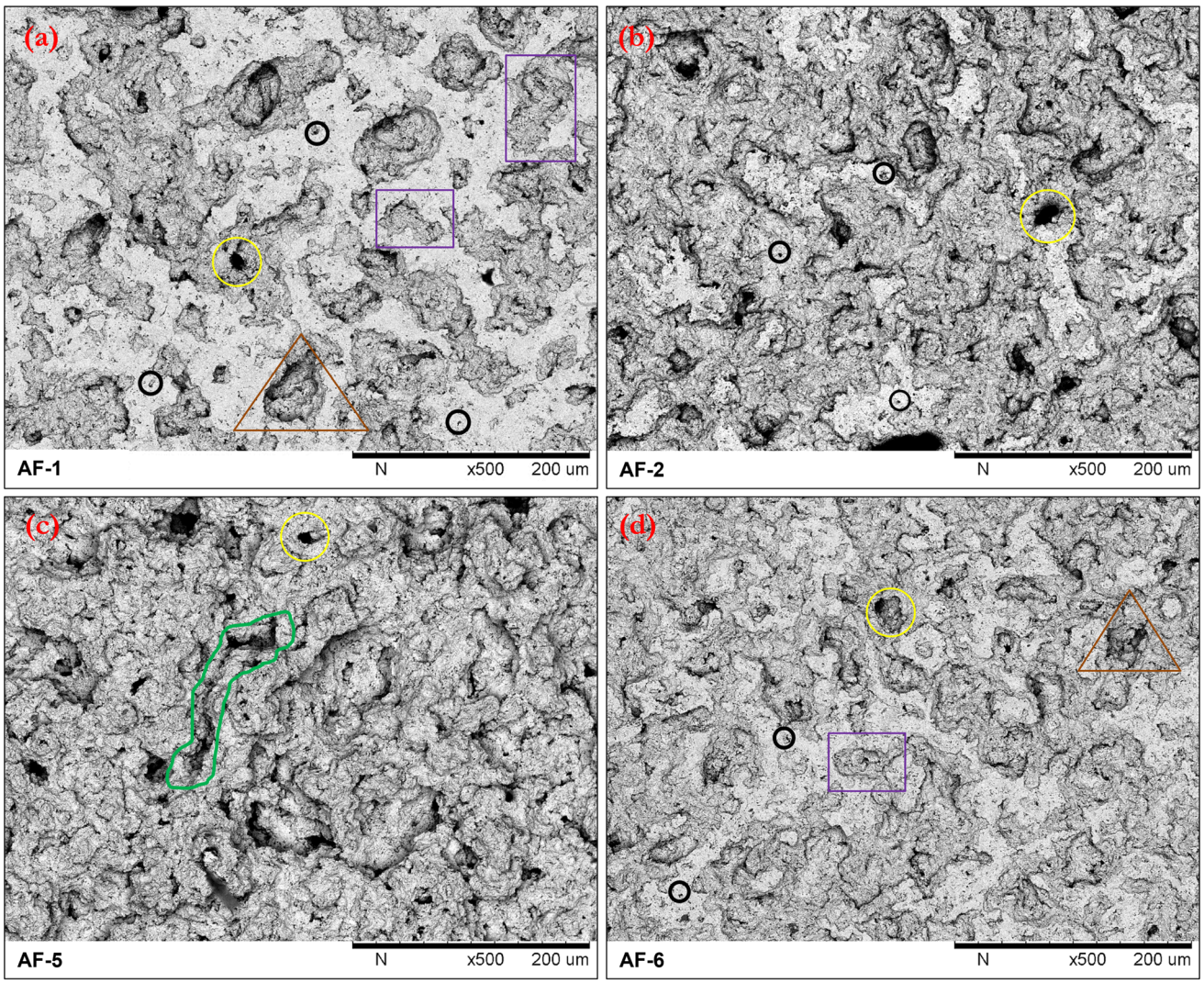


Fig. 14 SEM micrograph of the cavitation erosion evaluated HVOF coating and the thick HVAF coatings showing different surface damage features—the black outlined circles depict the least damaged regions, the yellow outlined circles depict the micron size pits, the large rectangles depict the mild eroded, the triangle depicts the severely eroded region while the most damaged part of the surface is represented by a trench-like pit marked by a free-form shape—(a) coarse powder deposited with 4L2 nozzle (b) coarse powder deposited with 5L4 nozzle (c) fine powder deposited with 3L0F nozzle (b) fine powder deposited with 3L3F nozzle

spray deposition conditions aided by microstructural analysis of the tested surface to show the damaged features created by the test conditions. SEM micrographs showing the post-cavitation erosion features of the coatings are presented in Fig. 14. There were four main damage features: the least damaged regions contained submicron pits marked by black outlined circles, micron-sized pits marked by yellow outlined circles, mildly eroded regions marked by large rectangles, and severely eroded regions marked by a triangle. The most damaged part of the surface is represented by a trench-like pit marked by a free-form shape. The individual coatings exhibited some or all the identified features as a mark of their cavitation erosion resistance. The most resistant of the coatings, AF-6, had a mildly eroded region mixed with sub-micron pit regions. The least resistant of the tested coatings, AF-5, lost all its submicron pit regions; it also presented a trench-like pit across its surface, confirming the aggressive material loss it experienced. Matikainen et al. (Ref 24) studied the cavitation erosion resistance of WC-CoCr deposited by high velocity spray processes. They found that the particle temperature and velocity affected the resistance of the coating to

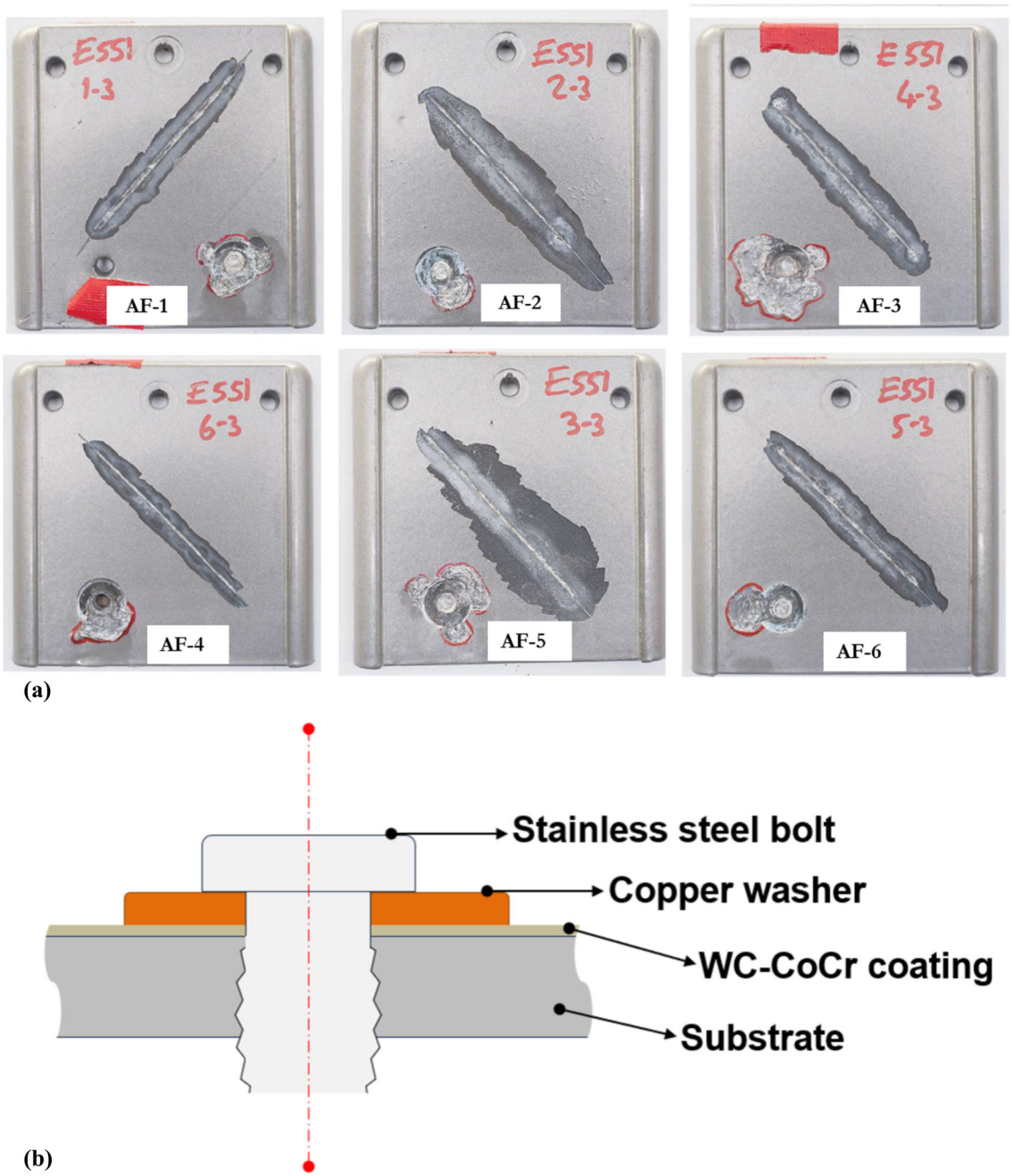


Fig. 15 (a) Camera image of the top surface of corrosion-tested samples showing two corrosion regions—scribed lines to create an exposed surface and steel bolt/copper washer assembly for galvanic activity. (b) Schematic representation of corrosion-tested samples showing the steel bolt/copper washer assembly on the WC-CoCr coated substrate for galvanic activity

cavitation erosion. Coatings deposited at high impact velocities resisted cavitation erosion better than those deposited at elevated temperatures and reduced impact velocities. This observation explains the erosion rate of the coatings. Two of the four HVAF coatings, AF-2 and AF-6, deposited under a spray condition of high impact velocity, demonstrated the best resistance to cavitation erosion. These results suggest that the spray conditions play a significant role in determining the cavitation resistance of coatings with respect to the powder cut size. This suggests that either of the two powders used for HVAF spraying can produce cavitation-resistant coatings if the spray parameters are optimized.

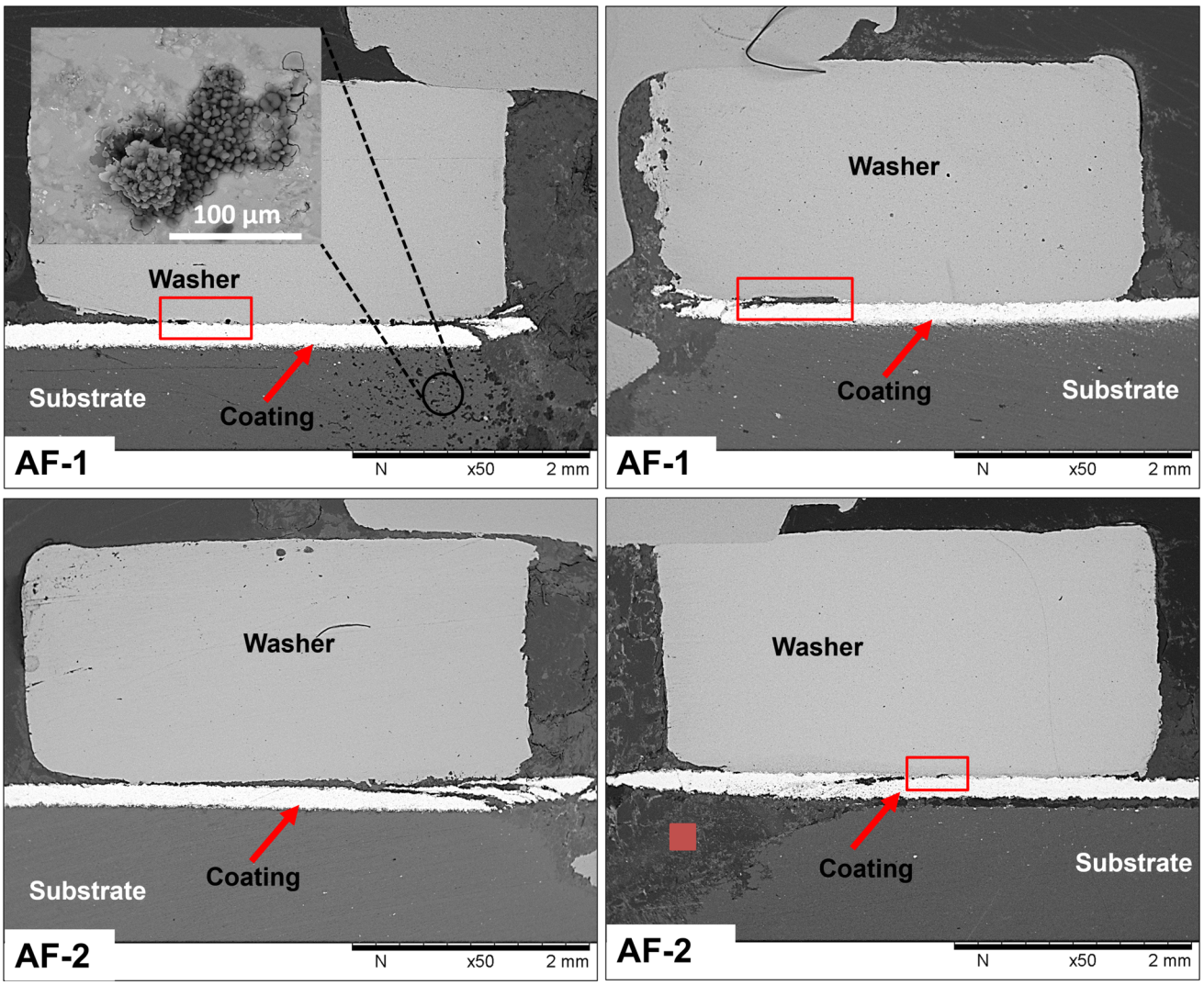
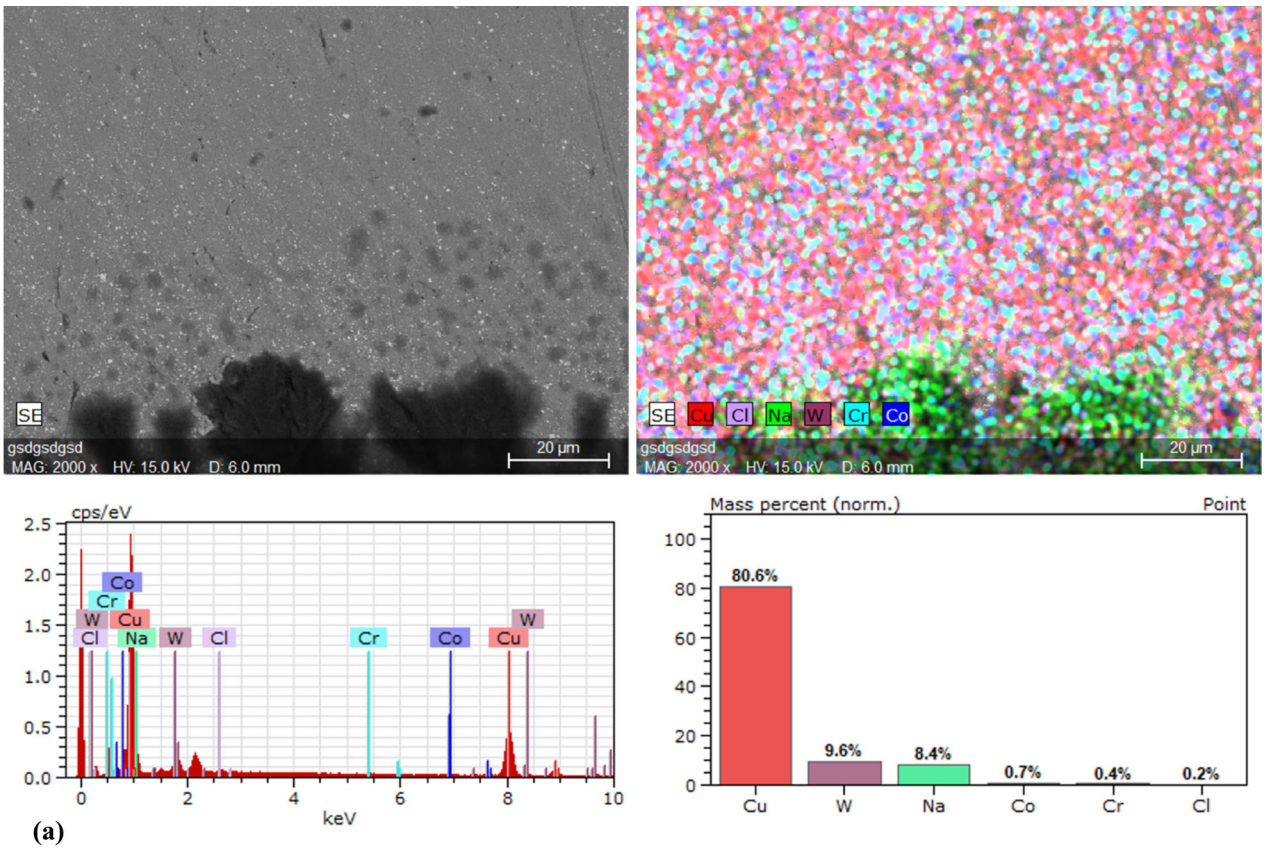


Fig. 16 Scanning electron micrographs showing the cross-sectional view of the combined halves of the corrosion-tested samples for AF-1 and AF-2 coatings with an inset showing the pitting sites on the substrate. The red outlined box shows the crevice corrosion site, while the filled square dot represents the corrosion-degraded region of the substrate analyzed by EDX

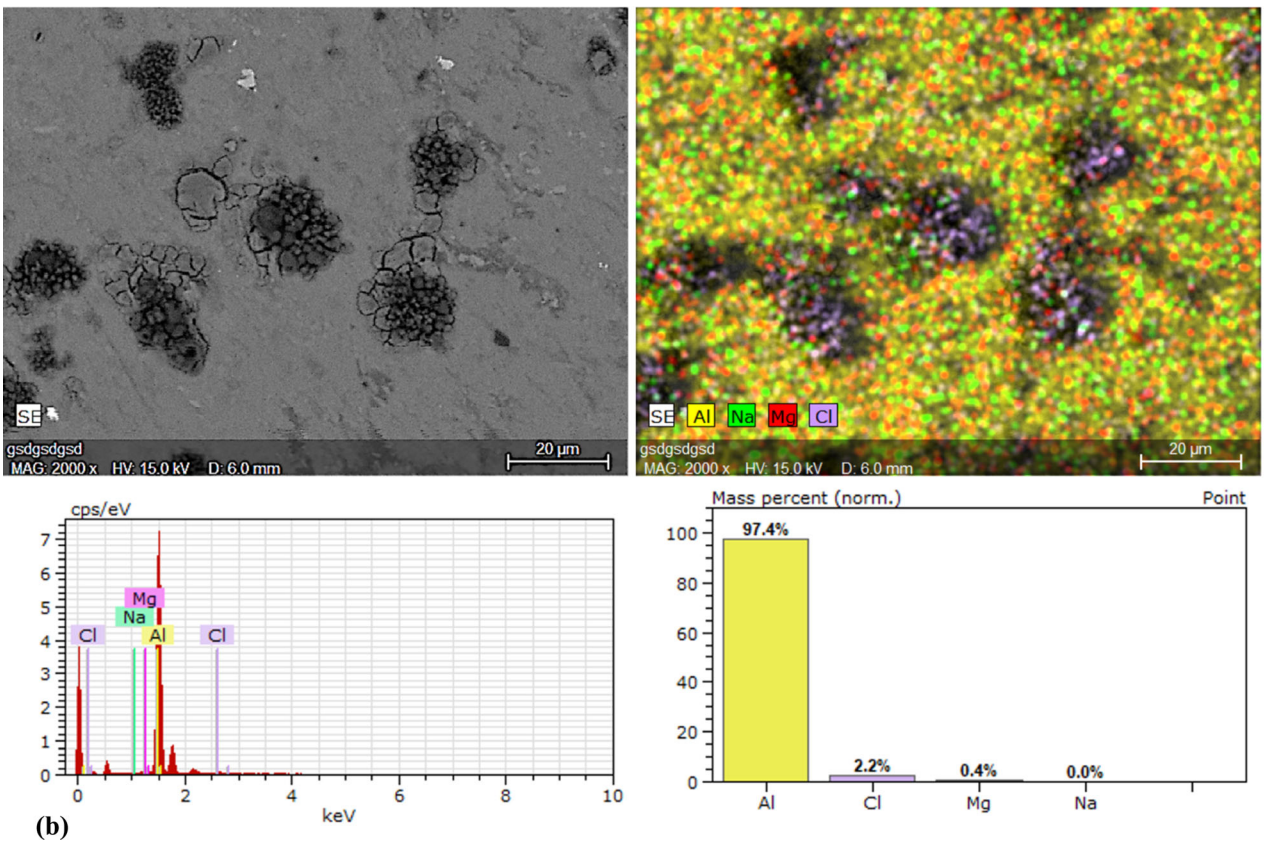
Corrosion in Synthetic Atmosphere

A microstructural study of the coating samples exposed to synthetic atmospheric corrosion was conducted using scanning electron microscopy with EDX analysis. The microstructural features obtained suggest that three different corrosion mechanisms facilitated the degradation of the samples under simulated atmospheric conditions. The camera images of the tested samples are presented in Fig. 15(a), which shows the top-surface conditions of the samples after a 16-week exposure period. Each sample showed signs of corrosion between the coating and the topcoat paint in the unprotected diamond-marked region. There is also clear evidence of corrosion activity near the bolt/washer assembly regions on each of the samples to varying degrees. However, the top surface image does not reveal whether the corrosion damage is restricted to the underlying coatings or reaches the washer, the stainless steel bolt, or the aluminum alloy substrate. A cross-sectional view of the tested samples provided insight into the depth and nature of the degradation observed on the top surface—see the schematic representation in Fig. 15(b).

Cross-sectional views of the assemblies are shown in Fig. 16 and 18, respectively. Figure 16 presents the combined halves of the assemblies, showing the AF-1 and AF-2 coatings sprayed from the coarse WOKA 3654 powder.


SE
gsdgsdgsd
MAG: 2000 x HV: 15.0 kV D: 6.0 mm
20 µm
SE Cu Cl Na W Cr Co
gsdgsdgsd
MAG: 2000 x HV: 15.0 kV D: 6.0 mm
20 µm
cps/eV
Co
Cr
W Cu
Cl Na W Cl
Cr
Co
Cu
W
keV
Mass percent (norm.)
Point
80.6%
9.6%
8.4%
0.7%
0.4%
0.2%
Cu
W
Na
Co
Cr
Cl

(a)


SE
gsdgsdgsd
MAG: 2000 x HV: 15.0 kV D: 6.0 mm
20 µm
SE Al Na Mg Cl
gsdgsdgsd
MAG: 2000 x HV: 15.0 kV D: 6.0 mm
20 µm
cps/eV
Mg
Na
Cl
Al
Cl
keV
Mass percent (norm.)
Point
97.4%
2.2%
0.4%
0.0%
Al
Cl
Mg
Na

(b)

◀**Fig. 17** (a) EDX analysis of crevice corrosion sites on tested samples showing elemental compositions and mass % of corrosion agents (Na and Cl) compared to other elements. (b) EDX analysis of pitting corrosion sites on tested samples showing elemental compositions and mass % of corrosion agents (Na and Cl) compared to other elements

The left and right halves of the assemblies are shown for each sample to present what happens on both sides of the stainless steel bolt. The post-corrosion test created interfaces and products from the interaction of the corrosion agents carried in the simulated rainwater with % 5 NaCl and the synthetic seawater with 5 % salinity, the coating, and the metals (the underlying substrate and the top washer). The corrosion features observed in the two samples consist of crevices and pitting corrosion sites. The pitting sites shown on the AF-1 assembly were on one side of the substrate, whereas the crevice sites were at the interface between the washer and the coatings on both sides. The source of the corrosion activity is the corrosion media penetrating the spaces between the assemblies. For AF-1, the corrosive media penetration created crevice corrosion sites between the coating and the washer, as shown by the red outlined boxes. There are also pitting sites on the substrates, as shown in the inset. Crevice and pitting sites were created because of the penetration of corrosive media from the space between the bolt and the substrate. There was no obvious path for the corrosive media directly from above the coating to the substrate. For AF-2, the corrosive media penetrated between the washer and the coating on one side and between the coating and the substrate on the other side; in both cases, the penetration of the corrosive media came from the space between the bolt and the other components of the assembly. EDX analysis of the crevice and pitting sites is shown in Fig. 17. The crevice site is shown in Fig. 17(a); its growth direction was away from the coating/washer interface, eating into the washer. The elemental composition of the crevice revealed the presence of sodium (Na, $\sim$ 8.4 %) and chlorine (Cl, $\sim$ 0.2 %). The crevice developed owing to the electropotential difference between copper and sodium in the cathodic and anodic states, respectively. The pitting sites represent localized corrosion sites on the Al substrate. The elemental analysis of the sites in Fig. 17(b) shows the presence of chlorine within the pit.

Microstructural images of the coatings developed from WOKA 3661FC are shown in Fig. 18, presenting samples AF-3 to AF-6. The degradation observed for all samples matched the degradation observed in the AF-1 and AF-2 samples. There were crevice sites across the samples, while AF-5 showed pitting degradation, as seen on AF-1. Much of the degradation on the substrates was below the coating, and it was traceable to the sipping in of the corrosive media through the bolt connection. The EDX analysis of the degraded sections of the substrate marked with the filled box points is presented in Fig. 19. The elemental composition of the region was Na ($\sim$ 1.2 %) and Cl ($\sim$ 7.1 %). The analyzed region also shows the presence of cracks, suggesting an additional mechanism for the observed corrosion—stress corrosion cracking.

Conclusions

Six HVAF-sprayed coatings deposited on both steel substrates and aluminum alloy substrates using two separate WC-CoCr feedstocks and separate spray conditions alongside a standard HVOF-sprayed WC-CoCr were investigated for microstructure, microhardness, corrosion, dry sliding wear, dry sand abrasion wear, and cavitation erosion. The following conclusions were drawn:

- The HVAF coating deposited under the spray conditions that create a high impact velocity of the feedstock shows better sliding wear performance irrespective of the feedstock particle size range and spray parameters. The effect of the substrate was observed in the case of thinner coatings, where coatings on an aluminum substrate with lower hardness and yield strength exhibited a higher specific wear rate than coatings on a steel substrate.
- Coatings sprayed by HVAF with coarse-cut powder sprayed under conditions that create a high impact velocity show the best abrasion resistance.
- The cavitation erosion resistance of the thick HVAF coatings shows that suitable spray parameters could be identified to protect a surface against cavitation erosion irrespective of the feedstock particle size range.
- All the coatings demonstrated effective corrosion resistance, as there was no observed coating degradation under the simulated atmospheric and seawater conditions.

The results show that, in general, HVAF WC-CoCr coatings can impart the desired protection to the targeted steel and aluminum components in marine environments. The presented results suggest that the steel shaft and aluminum hub, in an application prone to sliding and abrasion wear, can be coated thickly using the HVAF spray technique with coarse-cut WC-CoCr powder, while the propeller, which is prone to sliding, abrasion, and cavitation-erosion wear, can be coated thick using the HVAF spray

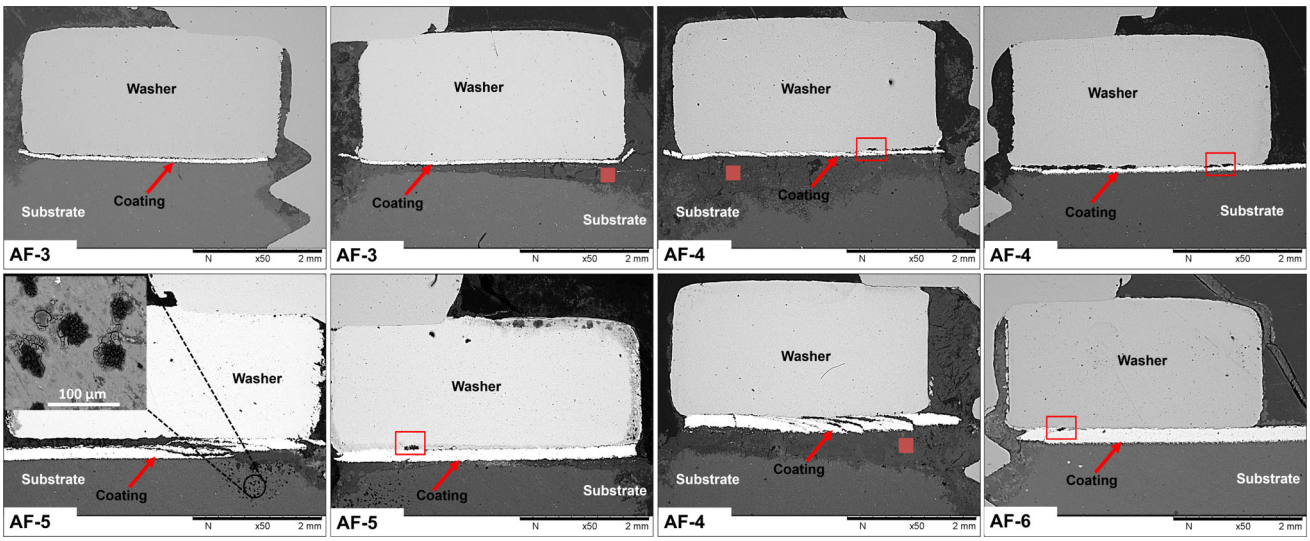


Fig. 18 Scanning electron micrograph showing the cross-sectional view of the combined halves of the corrosion-tested samples for AF-3 to AF-6 coatings with an inset showing pitting sites on the substrate—the red outlined box shows the crevice corrosion site, while the filled square dot represents the corrosion degraded region of the substrate analyzed by EDX

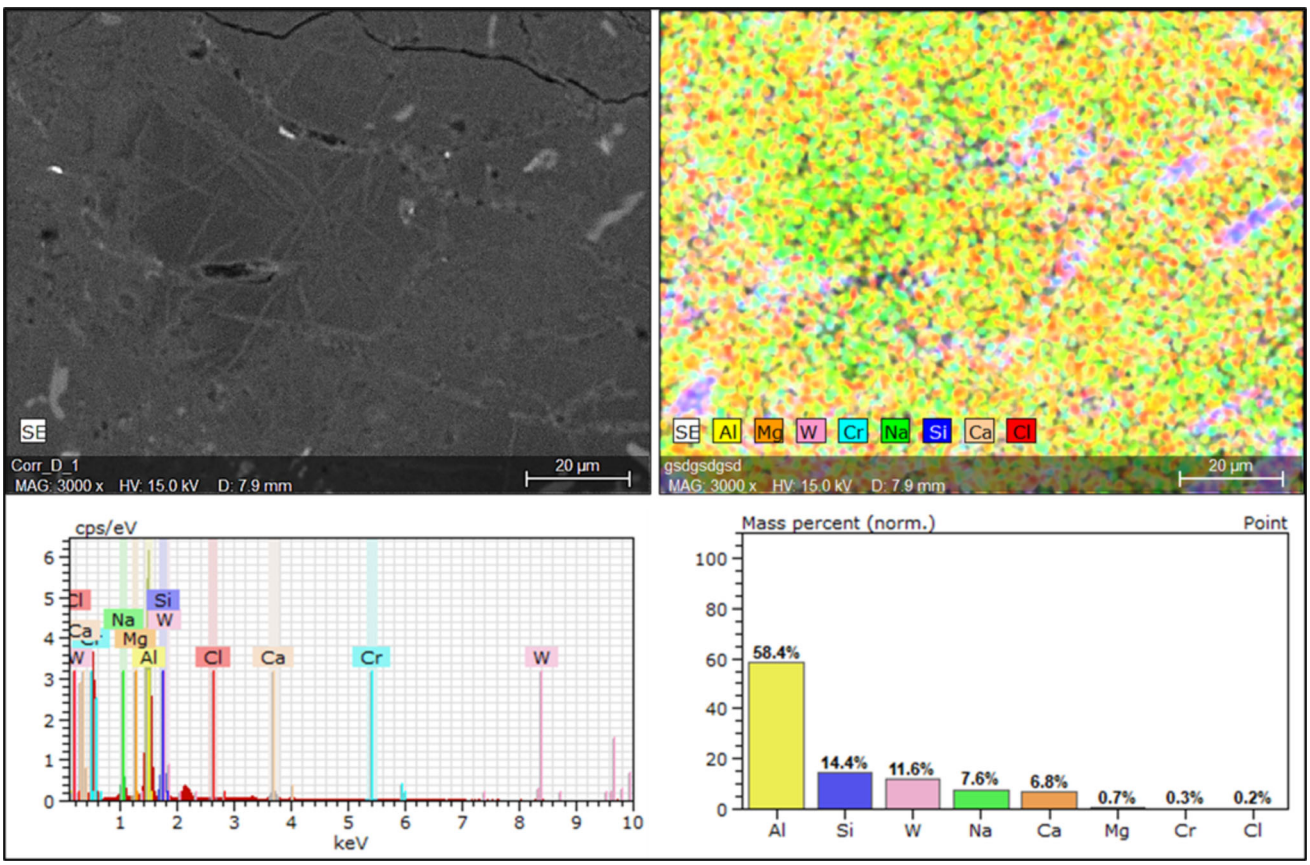


Fig. 19 EDX analysis of the corrosion-degraded regions on the substrates marked with filled square boxes on the cross sections in Figure 18. The elemental composition of the scanned region and the mass % of the corrosion agents (Na and Cl) were compared with those of the other elements

technique with fine-cut WC-CoCr powder for the best performance.

Acknowledgments This project was funded by the Swedish funding agency Vinnova (Reference number: 2021-04043), as part of the strategic innovation program LIGHTer. The authors would like to thank their colleagues at University West, Stefan Björklund, and Magnus Sandberg for their assistance in spraying the HVAF coatings. The authors also appreciate Olav Norheim of Thermal Spray Engineering (TSE) for performing HVOF deposition.

Funding Open access funding provided by University West.

Open Access This article is licensed under a Creative Commons Attribution 4.0 International License, which permits use, sharing, adaptation, distribution and reproduction in any medium or format, as long as you give appropriate credit to the original author(s) and the source, provide a link to the Creative Commons licence, and indicate if changes were made. The images or other third party material in this article are included in the article's Creative Commons licence, unless indicated otherwise in a credit line to the material. If material is not included in the article's Creative Commons licence and your intended use is not permitted by statutory regulation or exceeds the permitted use, you will need to obtain permission directly from the copyright holder. To view a copy of this licence, visit http://creativecommons.org/licenses/by/4.0/.

References

1. V. Haaja, T. Varis, J. Laurila, and M. Isakov, Fretting Behavior of WC-Co-Cr Coatings Against QT Steel in Bolted Joint, *J. Therm. Spray. Tech.*, 2024, **33**, p 1117.
2. M. Dular and M. Petkovšek, On the Mechanisms of Cavitation Erosion—Coupling High Speed Videos to Damage Patterns, *Exp. Therm. Fluid Sci.*, 2015, **68**, p 359-370.
3. V. Singh, V. Kumar, A. Bansal, A.K. Singla, and R. Verma, Corrosion-Cavitation Erosion Improvement of Marine Steel by High-Velocity Oxy-Fuel-Sprayed Vanadium Carbide Coatings and Polytetrafluorethylene Topcoat, *J. Mater. Eng. Perform.*, 2024 https://doi.org/10.1007/s11665-024-09711-0
4. A.G. Lekatou, D. Sioulas, and D. Grimanelis, Corrosion and Wear of Coatings Fabricated by HVOF-Spraying of Nanostructured and Conventional WC-10Co-4Cr Powders on Al7075-T6, *Int. J. Refract. Met. H*, 2023, **112**, p 106164. (**in English**)
5. Y. Liu, T.E. Fischer, and A. Dent, Comparison of HVOF and Plasma-Sprayed Alumina/Titania Coatings—Microstructure, Mechanical Properties and Abrasion Behavior, *Surf. Coat. Technol.*, 2003, **167**(1), p 68-76.
6. R.S. Lima and B.R. Marple, From APS to HVOF Spraying of Conventional and Nanostructured Titania Feedstock Powders: A Study on the Enhancement of the Mechanical Properties, *Surf. Coat. Technol.*, 2006, **200**(11), p 3428-3437.
7. J. Eklund, J. Phother, E. Sadeghi, S. Joshi, and J. Liske, High-Temperature Corrosion of HVAF-Sprayed Ni-Based Coatings for Boiler Applications, *Oxid. Met.*, 2019, **91**(5), p 729-747.
8. J. Kawakita, S. Kuroda, T. Fukushima, H. Katanoda, K. Matsuo, and H. Fukanuma, Dense Titanium Coatings by Modified HVOF Spraying, *Surf. Coat. Technol.*, 2006, **201**(3), p 1250-1255.
9. K. Torkashvand, M. Gupta, S. Björklund, F. Marra, L. Baiamonte, and S. Joshi, Influence of Nozzle Configuration and Particle Size on Characteristics and Sliding Wear Behaviour of HVAF-Sprayed WC-CoCr Coatings, *Surf. Coat Tech.*, 2021, **423**, p 127585. (**in English**)
10. J. Pulsford, S. Kamnis, J. Murray, M. Bai, and T. Hussain, Effect of Particle and Carbide Grain Sizes on a HVOAF WC-Co-Cr Coating for the Future Application on Internal Surfaces: Microstructure and Wear, *J. Therm. Spray Technol.*, 2018, **27**(1), p 207-219.
11. K. Bobzin, W. Wietheger, E. Burbaum, L.M. Johann, L.J. Rempe, V. Matikainen, U. Kanerva, M. Karhu, J. Lagerbom, K. Kaunisto, and J.F. Lartigue, Investigation of novel Nano-Carbide WC/CoCr Coatings Applied by HVAF, *J. Therm. Spray Technol.*, 2023, **32**(6), p 1772-1779. (**in English**)
12. T. Bellezze, G. Roventi, and R. Fratesi, Localised Corrosion and Cathodic Protection of 17 4PH Propeller Shafts, *Corros. Eng. Sci. Technol. Int. J. Corros. Processes Corros. Control*, 2013, **48**(5), p 340-345.
13. H. Ge, J. Li, and H. Chen, Cavitation Noise from Elastic Response of Metals in Ultrasonic Cavitation Erosion, *Proc. Inst. Mech. Eng. Part J J. Eng. Tribol.*, 2015, **230**(7), p 836-841.
14. T. Lee, Improvement of Viscoelastic Damping in Nickel Aluminum Bronze by Indium-Tin, *Met. Mater. Int.*, 2011, **17**(3), p 425-430.
15. D.R. Lenard and J.G. Moores, Initiation of Crevice Corrosion by Stray Current on Stainless Steel Propeller Shafts, *Corrosion*, 1993, **49**(9), p 769-775.
16. X. Ding, Q. Wang, Y.H. Tian, C.C. Yang, C.Q. Yuan, and C.S. Ramachandran, Microstructure and Wear Performance of CeO2-Modified Micro-Nano Structured WC-CoCr Coatings Sprayed with HVOF, *Lubricants*, 2023, **11**(5), p 188. (**in English**)
17. A. Ghabchi, T. Varis, E. Turunen, T. Suhonen, X. Liu, and S.P. Hannula, Behavior of HVOF WC-10Co4Cr Coatings with Different Carbide Size in Fine and Coarse Particle Abrasion, *J. Therm. Spray Technol.*, 2010, **19**(1), p 368-377.
18. G. Bolelli, L. Lusvarghi, and M. Barletta, HVOF-Sprayed WC-CoCr Coatings on Al Alloy: Effect of the Coating Thickness on the Tribological Properties, *Wear*, 2009, **267**(5), p 944-953.
19. A.G. Fefekos, M. Gupta, S. Mahade, S. Björklund, and S. Joshi, Effect of Spray Angle and Substrate Material on Formation Mechanisms and Properties of HVAF Sprayed Coatings, *Surf. Coat. Technol.*, 2023, **452**, p 129115.
20. S. Morelli, G. Rombola, G. Bolelli, M. Lopresti, P. Puddu, E. Boccaleri, L. Seralessandri, L. Palin, V. Testa, M. Milanesio, and L. Lusvarghi, Hard Ultralight Systems by Thermal Spray Deposition of WC-CoCr onto AZ31 Magnesium Alloy, *Surf. Coat Tech.*, 2022, **451**, p 129056. (**in English**)
21. M. Parco, L. Zhao, J. Zwick, K. Bobzin, and E. Lugscheider, Investigation of HVOF Spraying on Magnesium Alloys, *Surf. Coat. Technol.*, 2006, **201**(6), p 3269-3274.
22. ASTM, Standard Test Method for Wear and Friction Testing with a Pin-on-Disk or Ball-on-Disk Apparatus G99-23, ASTM International, p. 6 (2017)
23. ASTM, Standard Test Method for Measuring Abrasion Using the Dry Sand/Rubber Wheel Apparatus, ASTM International, p. 14 (2021)
24. V. Matikainen, S.R. Peregrina, N. Ojala, H. Koivuluoto, J. Schubert, S. Houdková, and P. Vuoristo, Erosion Wear Performance of WC-10Co4Cr and CrC-25NiCr Coatings Sprayed with High-Velocity Thermal Spray Processes, *Surf. Coat. Technol.*, 2019, **370**, p 196-212. (**in English**)
25. G. Bolelli, L.M. Berger, T. Börner, H. Koivuluoto, L. Lusvarghi, C. Lyphout, N. Markocsan, V. Matikainen, P. Nylén, P. Sassatelli, R. Trache, and P. Vuoristo, Tribology of HVOF- and HVAF-Sprayed WC-10Co4Cr Hard Metal Coatings: A Comparative Assessment, *Surf. Coat. Technol.*, 2015, **265**, p 125-144.
26. A. Lekatou, D. Sioulas, A.E. Karantzalis, and D. Grimanelis, A Comparative Study on the Microstructure and Surface Property

Evaluation of Coatings Produced from Nanostructured and Conventional WC-Co Powders HVOF-Sprayed on Al7075, *Surf. Coat. Technol.*, 2015, **276**, p 539-556.
27. F.R. Caliari, F.S. Miranda, D.A.P. Reis, G.P. Filho, L.I. Charakhovski, and A. Essiptchouk, Plasma Torch for Supersonic Plasma Spray at Atmospheric Pressure, *J. Mater. Process. Technol.*, 2016, **237**, p 351-360.
28. J. Cizek, I. Dlouhy, F. Siska, and K.A. Khor, Modification of Plasma-Sprayed TiO2 Coatings Characteristics via Controlling the in-Flight Temperature and Velocity of the Powder Particles, *J. Therm. Spray Technol.*, 2014, **23**(8), p 1339-1349.
29. A. Garfias Bulnes, V. Albaladejo Fuentes, I. Garcia Cano, and S. Dosta, Understanding the Influence of High Velocity Thermal Spray Techniques on the Properties of Different Anti-Wear WC-Based Coatings, *Coatings*, 2020, **10**(12), p 1157.
30. L. Jacobs, M.M. Hyland, and M. De Bonte, Comparative Study of WC-Cermet Coatings Sprayed via the HVOF and the HVAF Process, *J. Therm. Spray Technol.*, 1998, **7**(2), p 213-218. (**in English**)
31. Y. Liu, W. Liu, Y. Ma, S. Meng, C. Liu, L. Long, and S. Tang, A Comparative Study on Wear and Corrosion behaviour of HVOF—and HVAF-Sprayed WC-10Co-4Cr Coatings, *Surf. Eng.*, 2017, **33**(1), p 63-71.
32. K. Torkashvand, M. Gupta, S. Björklund, and S. Joshi, Tribological Performance of Thin HVAF-Sprayed WC-CoCr Coatings Fabricated Employing Fine Powder Feedstock, *J. Therm. Spray Technol.*, 2022, **32**(4), p 1033-1046.
33. K. Torkashvand, S. Joshi, V. Testa, F. Ghisoni, S. Morelli, G. Boleli, L. Lusvarghi, F. Marra, and M. Gupta, Tribological Behavior of HVAF-Sprayed WC-Based Coatings with Alternative Binders, *Surf. Coat. Technol.*, 2022, **436**, p 128296. (**in English**)
34. A.K. Krella, Degradation and Protection of Materials from Cavitation Erosion: A Review, *Materials (Basel)*, 2023, **16**(5), p 2058. (**in English**)

Publisher's Note Springer Nature remains neutral with regard to jurisdictional claims in published maps and institutional affiliations.